CLM-P218

United Kingdom Atomic Energy Authority

RESEARCH GROUP

Preprint

COLLISIONLESS SHOCK WAVES

J. W. M. PAUL

Culham Laboratory
Abingdon Berkshire

1969

C O N T E N T S

PART I

A GENERAL REVIEW

1. RELEVANCE OF SHOCK STUDIES

1.1. Occurence of Shocks

The first upsurge of interest in plasma shock waves was stimulated by the possibility of heating ions rapidly to thermonuclear temperatures. Under these conditions the plasma and the shock would necessarily be free from classical binary collisions, that is collisionless. More recently, however, interest has centred on geophysical and astrophysical phenomena, in which the same collisionless conditions prevail.

A shock is produced by the rapid compression of a plasma and it necessarily results in energy dissipation, that is irreversible plasma heating. The non-classical heating mechanism involved in collisionless shocks has attracted much theoretical interest.

In the laboratory collisionless shocks have been observed in various experiments[1-13]. The pinch effect is frequently used to compress an initial plasma, and consequently to generate a cylindrically imploding shock. Non-cylindrical pinches, such as occur in very short pinch tubes[13], toroidal pinches[14], plasma guns[15] and plasma focus devices[16] also produce shocks. These various pinch devices are used in fusion research and as sources of electromagnetic and neutron radiation. Simulation of geophysical shocks has been performed in a plasma wind tunnel driven by a special arc source[8]. Some early plasma shock studies were performed using electromagnetic shock tubes of both 'T'[17] and annular geometry[18].

In the field of geophysics, satellite observations have shown that the earth's magnetosphere is embedded in a supersonic flow of plasma from the sun, but protected from it by a collisionless bow shock,[19] as shown in Fig.1. Such observations have also demonstrated the correlation between terrestrial magnetic storms and interplanetary shock waves[20] travelling through the solar wind (Fig.2). These satellite observations have involved a considerable expenditure of scientific effort and money and have given rise to a large number of theoretical papers on collisionless shock phenomena[21-26].

In addition to the above observations of collisionless shocks, there are many theories, or speculations, which involve collisionless shock waves in solar and astrophysical contexts. Three types of shock are currently thought to occur in connection with solar flares: (i) the flow pattern of plasma and magnetic field near the magnetic neutral point is thought to involve a slow shock front[27], (ii) the explosive release of energy in the

flare gives rise to a shock wave travelling over the surface of the sun which has been observed[28] through the radio emission from the hot electrons; and (iii) another shock[29] travels out into the solar wind along the open magnetic field lines emanating from the flare (Fig.3).

In the more distant and speculative areas of astrophysics, there are various examples of explosive plasma events which are thought to involve shock waves. Some models of radio sources[30], quasars[30] and pulsars[31] have invoked shock phenomena (e.g. Fig.4). The best known explosive event, the supernova, is generally accepted as involving some sort of expanding shock wave.

1.2. Theoretical Significance

Until recently, most theoretical plasma physics has been concerned with understanding the great variety of small amplitude (linear) waves and their rleated linear instabilities. Attention is now moving on to waves of appreciable amplitude and the consequent modifications to the instabilities. A whole new range of non-linear phenomena occur, such as limitation of instability and turbulence. Shock waves physics can be regarded as an extension of the existing wave studies into the non-linear regime, where a wealth of new plasma physics is to be found.

The most important type of shock, the collisionless shock, is dependent of plasma turbulence, rather than collisions, for its heating mechanism. This shock provides a convenient opportunity to study plasma turbulence, which is in itself of importance in many branches of plasma physics. In particular, some laboratory collisionless shocks appear to be dominated by microturbulence driven by a universal instability[32]. This type of instability is of importance in plasma containment experiments. Thus shock wave experiments may provide a testing ground for non-linear and turbulent plasma theories.

2. NATURE OF THE SHOCK TRANSITION

2.1 Gas-Dynamic Shock

Before considering the problem of the plasma shock, it is useful to consider the much simpler gas-dynamic shock. Compression of a gas results in the propagation of a sound wave. This wave propagates by reason of the binary collisions in the gas. The velocity of these waves increases with compression. Consequently, for a finite amplitude, successive parts of the compression overtake each other, resulting in a steepening of the front. However, unless the compression is sufficiently rapid, e.g. its velocity is greater than the sound velocity, the wave is damped before it steepens.

This steepening process can be seen in terms of the simple dispersion curve of frequency ω against wave number $k = 2\pi/\lambda$. This is a straight line for a gas. The non-linearity, resulting from the finite amplitude, produces harmonics ($\sin^2 \omega t \rightarrow \cos 2\omega t$), which results in higher k, i.e. shorter wavelength and steepening. This steepening process is limited by viscous dissipation (irreversible heating) in the finite velocity gradient of the front. This dissipation is the non-linear consequence of the collisions which caused the wave to propagate in the first instance. The diffusive aspect of the viscous transport process balances the non-linear steepening. This balance occurs, and a steady state shock results, when the transport process provides sufficient dissipation to satisfy the steady conservation of mass, momentum and energy across the shock front. The conservation relations, called the Rankine-Hugoniot jump conditions[33], are independent of the mechanism of the shock front, which can be treated as a discontinuity.

The detailed structure of the shock front can be considered in terms of the fluid equations, using the Navier-Stokes approximation. Such calculations give a width for strong shocks which is of the order of the collision mean free path. This implies that the fluid equations are invalid, and the full kinetic equations should be used. Attempts have been made to construct kinetic solutions, but no completely satisfactory answer has been obtained. However, there is general agreement between both fluid and kinetic treatments and experimental results.

In gas dynamics, if there are no collisions there are no sound waves, and consequently no shock waves; the particles just interstream. Plasma physics has always leaned very heavily on gas dynamics for its models and concepts. Consequently, it was at one time throught that it would be impossible to create a plasma shock wave in the absence of classical binary collisions.

2.2. Collisions in a Plasma

Before discussing collisionless shocks, it is essential to have a clear concept of 'collisions' in a plasma. Plasma physics essentially involves solutions of the many-body problem which results from the long range Coulomb forces. There are few truly binary collisions in a plasma. Particles are deflected stochastically in the fluctuating electric fields of many other particles. This problem has usually been tackled by reducing the many-body interactions to an effective binary one. This allows the use of normal gas-dynamic fluid and kinetic concepts in plasma physics.

In a plasma the range of the interactions is limited by Debye screening, and this facilitates an approximation to binary oscillations. On the classical plasma model, a collision

occurs when a series of small angle deflections, calculated assuming a succession of binary collisions between un-correlated centres of a Debye screened Coulomb field, results in a 90^{o} deflection. Because of the screening term, this is equivalent to considering only collisions with impact parameters less than the Debye distance (λ_D).

This classical collision frequency can also be derived from the stochastic deflection of particles in the random fluctuating electric field of the thermal plasma. Fluctuating fields with $\lambda < \lambda_D$ originate in the incoherent thermal motions of single particles, while fluctuations with $\lambda > \lambda_D$ arise from the collective screening effects of many particles. The latter can be analysed conveniently into coherent waves. The classical collision approximation corresponds to neglecting these collective fluctuations. For a plasma in thermal equilibrium the ratio of the collective to the classical collision frequency is about $(0{\cdot}4/\ln \Lambda)$, where Λ is the Coulomb logarithm. This ratio is usually negligibly small, so that the classical approximation is valid.

However, real plasmas are rarely in thermal equilibrium. There is usually free energy present in the various gradients (density, magnetic field, velocity, temperature), currents, differences of temperature between particles or non-Maxwellian distribution functions. Some aspects of this non-equilibrium character can frequently interact with the low level of thermal waves in the plasma. This interaction is usually a resonance plasma instability which causes these waves to grow to a non-negligible level. The non-linear phase of this growth usually results in plasma turbulence. These collective fluctuating electric fields with $\lambda > \lambda_D$ produce stochastic particle deflections and lead to an effective binary collision frequency and transport coefficients, just as did the fluctuations with $\lambda < \lambda_D$. Such collective transport processes are usually called anomalous, turbulent or supra-thermal. Anomalous transport coefficients are usually invoked to explain experiments rather than derived theoretically. The latter requires sufficient knowledge of the non-linear phase of instability for the spectrum $\langle E^2(\omega, k)\rangle$ to be predicted.

The wide range of possible plasma instabilities within collisionless shocks is beyond this lecture, but some of the more important, e.g. the two-stream[32,34] and ion-acoustic[34-36] instabilities, will be discussed later.

This generalization of transport coefficients to include collective effects extends the useful range of the fluid model of a plasma, but it has one serious limitation. The classical binary approximation automatically gives rise to particle heating. The collective processes cause the growth of waves. The heating results finally from the damping of these waves. Thus there is an additional energy term in the system, corresponding to the energy

in these waves. If this energy is small compared with other energies in the system, as is often the case, then the fluid model is a reasonable approximation. The complete process described above results, as would be expected, in the conversion of the available free energy into random thermal energy.

2.3. Plasma Shock

Compression of a plasma can produce longitudinal waves (plasma sound waves), but in the presence of a magnetic field transverse non-compressional and mixed longitudinal and transverse waves are also possible. These waves occur even in the absence of classical binary collisions and are the result of the collective plasma effects. As in the case of the gas-dynamic shock the dispersion usually starts linearly, and such waves can steepen as the amplitude is increased forming the usual shock discontinuity. In a plasma this steepening can be limited by two different types of process, dissipation and dispersion.

(a) Dissipative Limitations. Dissipation occurs as in gas-dynamics, but now involves more transport coefficients because there are two types of particles and a magnetic field. Also both classical and collective transport are possible.

For a steady-state shock the conservation relations and Maxwell's equations must be satisfied. The resulting jump conditions are called the de Hoffmann-Teller relations[37], and these specify the required dissipation within the shock. Consider a simple case of a shock propagating perpendicular to a magnetic field. The jump conditions ($1 \rightarrow 2$) in the shock frame are the same as the Rankine-Hugoniot condition but with magnetic terms added to the pressure and internal energy:

$$\left.\begin{aligned} p^* &= p + B^2/(2\mu_o) \\ E^* &= E + B^2/(2\mu_o\rho) \end{aligned}\right\} \quad \text{(M.K.S. units)}$$

The conservation equations are listed below:

Mass: $$\rho_1 v_1 = \rho_2 v_2$$

Momentum: $$(v_1 - v_2)^2 = (p_2^* - p_1^*)(1/\rho_1 - 1/\rho_2)$$

Energy: $$E_2^* - E_1^* = \left(\frac{1}{\rho_1} - \frac{1}{\rho_2}\right)\left(\frac{p_1^* + p_2^*}{2}\right)$$

State: $$E = p/(\Upsilon - 1)$$

Maxwell: $$v_1 B_1 = v_2 B_2$$

Further simplifying to the case of a negligible ratio of initial particle to magnetic pressure ($\beta_1 \ll 1$), these reduce to a quadratic relation between shock strength $S = p_2^*/p_1^*$

and compression $F = \rho_2/\rho_1$

$$\left(\frac{\Upsilon-2}{\Upsilon-1}\right)F^2-\left(\frac{S+3}{2}\right)F+\frac{(\Upsilon+1)S+(\Upsilon-1)}{2(\Upsilon-1)}=0\ .$$

All other parameters can be obtained from F and S, for example the Alfvén Mach number,

$$M_A=\sqrt{\frac{F(S-1)}{2(F-1)}}$$

and the temperature behind the shock is given by

$$kT_2=\frac{B_1^2}{2\mu_0 n_1}\left(\frac{S-F^2}{F}\right)\ .$$

The more general cases are treated in Ref.38.

(b) Dispersive Limitation. Two characteristic forms of plasma dispersion curves are shown in Fig.5. If the steepening is limited by dissipation before the change of gradients of the dispersion curve, then a normal dissipative shock is formed. In the absence of such dissipation, steepening of the shock is limited by the nature of the dispersion curves. At the higher harmonics the phase velocity changes.

In case (a) the phase velocity of the wave decreases as the wave steepens. The higher harmonics, shorter wavelengths, are left behind, forming a set of compression oscillations behind the main front. This type of dispersion occurs for (i) wave propagation perpendicular to a magnetic field in a low β plasma as a result of electron inertial resonance at $\omega \sim \sqrt{(\omega_{ce}\omega_{ci})}$ and $(1/k) \sim (c/\omega_{pe})$ and (ii) an unmagnetized plasma at $\omega \sim \omega_{pi}$ and $(1/k) \sim \lambda_D$ from the ion plasma resonance.

In case (b) the same processes occur, but the phase velocity is now increasing and consequently the high frequency short wavelengths move in front of the main shock, forming a set of rarefaction oscillations. This second type of dispersion occurs for oblique propagation at an angle θ to the magnetic field in a low β plasma as a result of ion gyration in the whistler mode at $\omega \sim \omega_{ci}$, $(1/k) \sim \cos\theta(c/\omega_{pi})$.

Neither of these cases results in the formation of a shock. It is possible to add the energy of these oscillations to the energy equation and thereby satisfy the shock jump relations. But there is no real dissipation. These oscillations can be damped, either by classical or collective effects, to produce a damped wave train either behind or in front of the main jump, as shown in Fig.5. Clearly the forward wave train could not exist without such damping. Sometimes such damped oscillatory shock structures are called collisionless, because collisionless dispersion dominates, irrespective of the nature of the damping.

3. MHD CLASSIFICATION OF SHOCKS

Shocks have been classified on the one fluid MHD model by the nature of the jump conditions without reference to the structure[38]. The conservation equations of normal and transverse momentum, together with the energy equation (all including magnetic field effects), form three intercepting surfaces in a three-dimensional diagram with axes of temperature transverse magnetic field, and specific volume. In general these three surface intersect at four points, labelled 1, 2, 3, 4 in order of increasing compression. These intercepts are possible end points for a shock jump, which must occur from a lower to a higher number for entropy increase. These points are also divided in the middle by the initial Alfvén velocity appropriate to the magnetic field component in the direction of shock propagation. This leads to the following classification of shocks:

(a) fast or super-Alfvenic shocks $1 \rightarrow 2$, which are observed in the laboratory and are known theoretically to be stable;

(b) intermediate shocks $1 \rightarrow 3$, $1 \rightarrow 4$, $2 \rightarrow 3$, $2 \rightarrow 4$, which have not been observed and are thought theoretically to be unstable;

(c) slow shocks $3 \rightarrow 4$, which have not been observed but are thought to be stable;

(d) the transition points between fast and intermediate, and between intermediate and slow, shocks correspond to Switch On and Switch Off shocks respectively; and these have uncertain stability.

All subsequent discussion will be limited to fast shocks.

The existence of end points for a shock jump does not imply the existence of a continuous solution of the equations from the starting point to the final point. The jump conditions are independent of the mechanism, but the construction of a solution depends on the existence of suitable dissipation mechanisms to join the two points. This problem has been treated by means of the two fluid MHD equations. Fortunately, it is not necessary to solve the structure problem in order to prove the existence of the solution, because this is dependent only on the nature of the equations at the end-point singularities. Linear expansion of the equations about the singular points allows them to be classified as nodes, foci or saddles (Fig.6). This classification then determines whether solutions exist[39,40] between the two points (no entry into saddle), and if so, whether they are monotonic (node) or oscillatory (focus). Finally, after proving the existence of a solution, it is necessary to demonstrate the stability of this solution to small amplitude wave disturbances. This analysis[38] has shown that all fast shocks which exist, to which this discussion is limited, are stable.

4. MID SHOCK STRUCTURES

The shock structure problem requires the solution of the two-fluid equations of mass flow, momentum, energy, and state of the plasma together with Maxwell's equations through the shock. Complete analytical solutions are available only for very weak shocks propagating perpendicular to a magnetic field[41]. Strong shock solutions can be obtained analytically for certain simple cases[39,42-45] with a reduced number of transport processes (e.g. no thermoelectric effect). Computed solutions[46] tend to be for specific cases and lack detailed interpretation. There is much computational activity at present which should finds its way into the literature soon.

To illustrate the equations involved consider a simple case of a perpendicular shock in which the electrons and ions are shock-heated only by resistivity and viscosity respectively. Thermal conductivity, thermoelectric effects, electron inertia, etc. are ignored. In the frame of the shock, $v \equiv (v_x, 0, 0)$,

(a) Continuity: $nv = \text{const}$

(b) Momentum of ions or fluid:

$$Mnv \frac{dv}{dx} = J_y B_z - \frac{d(p_i + p_e)}{dx} + \frac{d}{dx}\left(\frac{4}{3}\mu \frac{dv}{dx}\right) \qquad \text{(x-component)}$$

(c) Momentum of electrons or generalized Ohm's Law:

$$neE_x = J_y B_z - \frac{dp_e}{dx} \qquad \text{(x-component)}$$

$$\eta J_y = (E_y - vB_z) - \frac{J_y B_z}{ne} \qquad \text{(y-component)}$$

(d) Energy equations:

(i) Ions $\frac{3}{2}nvk \frac{dT_i}{dx} = -p_i \frac{dv}{dx} + \frac{4}{3}\mu_i \left(\frac{dv}{dx}\right)^2$ (adiabatic and viscous heating)

(ii) Electrons $\frac{3}{2}nvk \frac{dT_e}{dx} = -p_e \frac{dv}{dx} + \eta J_y^2$ (adiabatic and resistive heating)

(e) Equation of state: $p = nkT$

(f) Maxwell's equations: $E_y = vB_z = v_1 B_{z1}$

$$J_y = -\frac{1}{\mu_o}\frac{dB_z}{dx}$$

In the shock problem the two important dissipative coefficients in the momentum equations are viscosity, associated with gradient of velocity; and resistivity, associated with the gradient of the magnetic field. Shocks can be classified as viscous or resistive, depending on which of these mechanisms dominates. Viscosity (μ) arises from interstreaming collisions, and for collision frequency ν is given by

$$\mu = nkT/\nu \quad (\propto T^{5/2} \text{ for classical collisions}).$$

The various combinations of inter-particle colllisions (e.g. ion-ion, electron-electron, ion-electron) each give rise to different viscosities (μ_{ii}, μ_{ee}, μ_{ie}). Resistance (η) arises from the relative motion of electrons and ions involved in a current flow and is given by

$$\eta = \left(\frac{m_e}{ne^2} \right) \nu \quad (\propto T^{-3/2} \text{ for classical collisions}).$$

One of the main differences in these two classes of shocks is the different dependence on ν. As the shock-heating depends on the product of the transport coefficient with the square of the appropriate gradient, there is a tendency for the resistive shock to steepen and for the viscous shock to broaden as ν decreases; that is with increasing temperature for classical collisions.

Thermal conductivity, another important transport coefficient does not appear directly in the momentum equation and cannot by itself support a strong shock but can modify the structure through the energy equation. Other phenomena, like the Hall effect and thermo-electric effect, can similarly modify the structure of the shock.

The most acceptable definition of the so-called 'collisionless' shock is that the irreversible shock heating in a 'collisionless' shock cannot be accounted for by using the classical transport coefficients in the fluid model.

The above fluid considerations apply to collective transport coefficients, provided always that these form a reasonable approximation. A shock in which such collective coefficients dominate, would be 'collisionless' although fluid-like.

5. CRITICAL MACH NUMBER FOR RESISTIVE SHOCKS

The previous discussion (Section 3) of the existence of continuous solutions between existing end points is high-lighted by the case of the resistive fast shock. Solutions joining the end points exist only below a certain critical Alfvén Mach number. There is no such limit if viscosity is present.

It is possible to produce a resistive shock in which viscous processes are negligible. For example, if the classical ion-ion mean free path is much longer than the characteristic compression length, or more simply the shock width, and no collective viscosity is present, then a purely resistive shock results. Above a critical Alfvén Mach number, resistivity alone cannot satisfy the conservation relations. As a result, a second steepening occurs within the resistive structure and this must be limited by a viscous process.

This critical Mach number is related to the existence of two Mach numbers in a magnetized plasma.

(a) The Alfvén Mach number ($M_A = V_S/V_A$), which relates the shock velocity (V_S) to the Alfvén velocity $[V_A = B/(\mu_0 nM)^{\frac{1}{2}}]$,[/] is relevant when the magnetic field is coupled to the compression.

(b) The acoustic Mach number ($M_S = V_S/C_S$), which relates V_S to the plasma sound speed (C_S), is relevant when there is no magnetic field or the field is uncoupled from the compression. In this case, if $M_S > 1$, steepening will lead to the formation of a viscous shock.

The value of C_S depends on the combination of adiabatic or isothermal sound speeds, $a = (\gamma kT/M)^{\frac{1}{2}}$ and $s = (kT/M)^{\frac{1}{2}}$ respectively, of the electrons and ions. For the collisionless resistive shock, the ions are adiabatic and the electrons isothermal, so that $C_S^2 = a_i^2 + s_e^2$.

On a scale-length short compared with the resistive shock-width, the magnetic field and plasmaare uncoupled. Consequently, if the local flow becomes acoustically supersonic, $M_S > 1$, acoustic waves will steepen forming a viscous shock as a steep jump near the rear of the resistive structure.

Above the critical Mach number, if there is no viscous process to limit the second steepening, the fluid equations break down by becoming multi-valued. This is usually interpreted to mean that the shock 'breaks' or 'overturns', producing interstreaming plasmas. This interstreaming and the resulting interstreaming instability, is thought to produce the required collective viscosity for these shocks to exist.

The critical Alfvén Mach number M_A^* for the appearance of this double structure, or for 'breaking', is obtained from the condition that the flow changes from acoustically super- to sub-sonic in passing through the shock (i.e. local $M_S = 1$). Thus M_A^* will depend on whether the electrons or ions are heated and whether they are adiabatic or isothermal. Woods[40] gives a consistent set of assumptions and values of M_A^* (Table I) which apply for collective as well as classical transport coefficients.

[/] Strictly, Alfvén waves do not exist for propagation perpendicular to B, but V_A is still used.

TABLE I

Critical Alfvén Mach numbers ($\beta_1 \ll 1$)

(k = thermal conductivity, η = resistivity, μ = viscosity)

	$\gamma = 5/3$		$\gamma = 2$	
Non-zero coefficient	$T_i = 0$	$T_i = T_e$	$T_i = 0$	$T_i = T_e$
k_e , k_i , $k_e + k_i$	1	1	1	1
η	2·76	2·76	2·95	2·95
$\eta + k_i$	2·76	3·01	2·48	2·80
$\eta + k_e$	3·46	3·01	3·56	2·80
$\eta + k_i + k_e$	3·46	3·46	3·56	3·56
μ + ...	∞	∞	∞	∞

6. NON-FLUID MODELS

6.1. Vlasov Treatment

The Vlasov equation considers changes of the particle distribution function produced by smoothed out electric and magnetic fields. These fields can clearly be analysed into plasma waves. Both analytical[35] and computational work[47,48] has been done in this field, but the description will be given in terms of the computational method. If the initial system is not in equilibrium (there is free energy), the initial smoothed out fields will change the initial distribution function of the particles in phase space. The resulting new average $(n_i - n_e)$ and current will then give the modified smoothed out fields, and so the calculation proceeds by steps. This method follows the resonant interactions of particles and waves.

In effect the computation is as follows:

(a) Instability: the interaction of particles with waves;

(b) Non-linear effects: wave decay, interaction of waves with waves, and scattering of waves on particles;

(c) Damping of waves and consequent heating of plasma.

The complete cycle transfers the free energy of the particles into thermal particle energy. The computational treatment is usually limited by the use of only one spatial dimension, a limited number of mesh points, and unrealistic m/M and λ_D. Up to the present, this method has not been applied to shock structures as a whole.

A similar, but more restricted, computation[21,23] has been performed using one-dimensional fluid sheets. The electron and ion fluids are coupled by the space charge

field. Distribution functions as such are not considered directly. Above M_A^* these sheets interpenetrate, but with certain assumptions the computation can be continued and interpreted. These computations have been performed for shocks in the realistic geometry of a theta-pinch.

6.2. Wave Kinetics

The recently developed wave kinetic model[49-51] provides an alternative approach which leans heavily on analogies with quantum mechanics. Instability, that is inverse Landau damping, is replaced by Cherenkov emission of a plasma wave quantum (phonon for ion wave and plasmon for electron wave) by the particle. The wave quanta make various quantum transitions; decay ($\omega_1 \rightarrow \omega_2 + \omega_3$), mutual wave-wave interactions ($\omega_1 + \omega_2 \rightarrow \omega_3 + \omega_4$), and interactions with particles (absorbing and scattering quanta, $\omega_1 + p_1 \rightarrow p_1'$ $\omega_1 + p_1 \rightarrow p_1' + \omega_2$). A formal quantum mechanical treatment is possible, but its use is limited by the difficulty of evaluating the transition probabilities.

7. PARAMETERS FOR THE CLASSIFICATION OF SHOCKS

It is difficult to make a clear classification of fast shocks. In this section the various parameters which, according to theory or experiment, affect the formation and nature of the structure will be listed with brief comments.

7.1. State of the Initial Plasma

(a) Degree of ionization : assume effectively fully ionized, (also state of ionization if $Z \neq 1$).

(b) Uniformity (e.g. n_e , B): affects dynamics of compression (e.g. axial gradients of n and B in θ-pinch tend to give non-cylindrical implosion).

(c) Quiescence/turbulence: macroscopic or microscopic (e.g. the solar wind appears to be turbulent).

(d) Mass or current flow: (e.g. compression of two interstreaming non-interacting plasmas).

7.2. Initial Plasma Parameters

(a) Presence or absence of magnetic field and ratio of particle to magnetic pressure.

$$\beta_e = \frac{n_e k T_e}{B^2/(2\mu_0)} = \left(\frac{S_e}{V_A}\right)^2 \quad ; \quad \beta_i = \frac{n_i k T_i}{B^2/(2\mu_0)} = \left(\frac{S_e}{V_A}\right)^2 \quad (\text{n.b. } n_e = n_i)$$

(b) Densities n_e , n_i and mass ratio m/M.

(c) Temperatures T_e , T_i and ratios T_e/T_i , $T_\parallel/T_\perp$. Distribution functions f_e , f_i if non-Maxwellian.

(d) Ratio Alfvén velocity (V_A) to the velocity of light (c) is important in that it is directly related to the ratios of characteristic frequencies

$$\frac{\omega_{ci}}{\omega_{pi}} = \frac{V_A}{c} \quad ; \quad \frac{\omega_{ce}}{\omega_{pi}} = \frac{M}{m}\left(\frac{V_A}{c}\right)$$

$$\frac{\omega_{ce}}{\omega_{pe}} = \left(\frac{M}{m}\right)^{\frac{1}{2}} \frac{V_A}{c} = \left(\frac{B^2}{\mu_o n m c^2}\right)^{\frac{1}{2}} = \alpha \quad ; \quad \frac{\lambda_D}{r_{ce}} \approx \alpha$$

In particular, if $\alpha > 1$, charge neutrality is violated over the electron orbit ($r_{ce} < \lambda_D$), which is then non-adiabatic. Also, if classical and collective collisions are negligible, the electron inertia waves of Section 2.3(b) have relativistic electron drift velocities.

7.3. Piston and Compression

(a) Geometry of piston in relation to magnetic field and any gradients. This determines geometry of shock.

(b) Stability and 'porosity' of the piston influence formation of separated shock.

(c) Relation of acceleration and steady phases to useful dimensions of apparatus influences formation of steady shock.

(d) Piston velocity influences Mach number.

7.4. Shock Conditions

(a) Clearly the values of the parameters listed in Section 7.2 can be important within the shock.

(b) A steady state, approximately plane shock front is desirable but not always achieved in experiments.

(c) The angle (θ) which the normal to the plane of the shock front makes with the magnetic field. Perpendicular ($\theta = \pi/2$), oblique ($0 < \theta < \pi/2$) or parallel ($\theta = 0$) shock.

(d) Mach numbers, Alfvén ($M_A = V_S/V_A$, acoustic ($M_S = V_S/C_S$) and magnetosonic $[M_M = V_S/(V_A^2 + C_S^2)^{\frac{1}{2}} = M_A/(1 + \frac{\gamma\beta}{2})^{\frac{1}{2}}]$ and relation to critical values.

(e) Is the observed shock structure (E, B, n)

(i) macroscopically steady and reproducible or turbulent?

(ii) montonic or oscillatory?

(iii) single or double?

(f) The ratio of shock width and rise time to characteristic lengths and times such as those of classical collisions λ_{ii}, τ_{ei}, gyro radii r_c, and $\lambda_D, (c/\omega_{pe})$, (c/ω_{pi}), ω_{ce}^{-1}, ω_{ci}^{-1}, $(\omega_{ce}\omega_{ci})^{-\frac{1}{2}}$, ..., etc.

(g) The conservation relations should be satisfied across the transition.

(h) Irreversible shock heating: strong or weak shock, electrons and/or ions heated.

(j) The ratio (R) of the observed to the calculated classical heating measures the importance of collective effects, that is, to what extent the shock is 'collisionless'. If $R > 1$, what type of instability is present and is there micro-turbulence ($\lambda \sim \lambda_D$) within the shock?

(k) Is the shock heated plasma thermal or tubulent?

8. REVIEW OF MAIN EXPERIMENTS AND RESULTS

The main laboratory experiments, summarized in Table II, will be reviewed briefly in relation to the present state of understanding. The various parameters measured and the diagnostic techniques used are summarized in Table III. The particular experiments with which the present author has been concerned are discussed in Part II of this chapter.

8.1. Perpendicular Shocks with low β_1 and $M_A < M_A^*$

In the absence of classical or collective collisions, such a shock would form a backward wave train of electron inertia oscillations, provided that $\alpha < 1$. A few heavily damped oscillations of this type with $\lambda \sim (c/\omega_{pe})$ have probably been observed[9,10].

For $\alpha > 1$ the electron current drift velocity (v_d) should, theoretically, become relativistic

$$v_d \sim \frac{1}{\mu_o ne}\frac{B}{L_s} \quad ; \quad L_s \sim \frac{c}{\omega_{pe}} \quad ; \quad \frac{v_d}{c} \sim \frac{B\omega_{pe}}{\mu_o nec^2} = \alpha \, .$$

Thus, if $\alpha > 1$, the shock width L_s must be greater than (c/ω_{pe}) and is given by

$$v_d \sim c \quad ; \quad L_s \sim \frac{B}{\mu_o nec} = \frac{V_A}{\omega_{pi}} \, .$$

Shocks of this type have probably been observed.[9]

The above structures are possible only if instabilities are absent. The most likely instability is the two-stream instability of the current[34]. This occurs if $v_d > v_{eth}$, the electron thermal velocity, and has a growth rate $\gamma \sim \omega_{pe}$. There is sufficient time[24] for this instability to grow in an electron inertia wave if

$$M_A > M_A' = 1 + \frac{3}{8}(\beta_1)^{\frac{1}{2}} \quad , \quad (\beta < 1) \, .$$

In the experiments mentioned above, these low Alfvén Mach numbers were obtained by using low densities and high magnetic fields. Above M_A', instability can be expected to damp out the oscillations, producing a monotonic structure. This change of structure has been observed experimentally[9].

The monotonic structure observed for $2 < M_A < 3$ is well documented on many different experiments. Universally $L_s \sim 10\,(c/\omega_{pe})$. Experiments show that the electrons, and not

TABLE II

SUMMARY OF PRINCIPAL EXPERIMENTS

Description	L_s
(I) In U.S.S.R.:	
1. Novosibirsk (Nesterikhin, Kurtmullaev, Alikhanov); Ref. 3,4,9	
(i) θ-pinch; $r = 8$ cm, $\beta_1 < 1$, various M_i	
(a) Perp.; $M_A < M_A^*$, below critical n_e^* oscillatory behind $\alpha > 1$	V_A/ω_{pi}(30 mm)
$\alpha < 1$	c/ω_{pe}(7 mm)
above n_e^* monotonic, anomalous η	10 c/ω_{pe}(15 mm)
$M_A > M_A^*$, double → mono, ion heating observed	c/ω_{pi}(30 mm)
(b) Oblique: $M_A < M_A^*$, oscillatory forward	$(\pi/2 - \theta)(c/\omega_{pi})$
$M_A > M_A^*$, double → mono	
No details of initial plasma, steadiness, B jump, separation or convergence.	
(ii) No B expt., 'VOLNA'; L = 100 cm; electron beam ionization, electrostatic piston	
(a) Weak, oscillatory	λ_D(20 mm)
(b) Strong	$10\lambda_D$
2. Moscow (Smolkin); θ-pinch UV - 1; $r = 3{\cdot}5$ cm; $\beta_1 < 1$; perp. shock; ref. 52,53	
$M_A < M_A^*$	$10c/\omega_{pe}$
$M_A > M_A^*$	c/ω_{pi}
(II) In U.S.A.:	
1. Austin (Robson, Sheffield); Loop θ-pinch; $r = 22$ cm, $\beta_1 < 1$; ref.13	
(a) Perp. on mid-plane, $M_A > M_A^*$, as TARANTULA (b) Oblique, $M_A < M_A^*$, oscillatory Detailed study of oblique steady state shock.	$\frac{2\pi \cos\theta}{(M_A^2 - 1)^{1/2}} \left(\frac{c}{\omega_{pi}}\right)$
2. Maryland (Hintz, de Silva, Goldenbaum)	
(i) Small θ-pinch; $r = 4{\cdot}5$ cm, $\beta < 1$; ref. 6, 54, 55 Non-steady perp. shock, T_e measurement gives $R \sim 1$ so may be classical collisions.	
(ii) Large θ-pinch; $r = 23$ cm, $\beta < 1$; ref. 12 $M_A < M_A^*$, Non-steady perp. shock, turbulent diffusion of piston	$3{\cdot}5\ (c/\omega_{pe})$
3. AVCO (Patrick, Pugh); 'TERRELLA' dipole expt; $L \sim 180$ cm, $\beta < 1$, $M_A < M_A^*$; ref. 8 Plasma wind tunnel from arc oblique not oscillatory, detailed study of fluctuation behind shock.	$(\frac{1}{2}\pi - \theta)\left(\frac{c}{\omega_{pi}}\right)$

TABLE II

continued

(III) In Germany:	
1. Julich (Hintz); Reverse field θ-pinch; r = 9 cm, $\beta_1 \gtrless 1$, perp. shock; ref.10	
(a) $\beta_1 < 1$, $M_A < M_A^*$; $M_A \sim 1{\cdot}3$, unsteady oscillation	$10(c/\omega_{pe})$
$M_A \sim 2{\cdot}4$, steady monotonic	$10(c/\omega_{pe})$
(b) $\beta_1 \sim 0{\cdot}5$; fluctuation behind shock ($\sim 10\ \omega_{ci}$);	
$M_A < M_A^*$	$10(c/\omega_{pe})$
$M_A > M_A^*$; no double structure for $M_A < 6{\cdot}5$	$0{\cdot}3(c/\omega_{pi})$
	$(20c/\omega_{pe})$
(c) $\beta_1 \sim 1$; fluctuation behind shock;	
$M_A \sim 8$	c/ω_{pi}
2. Garching (Keilhacker); θ-pinch; r = 7 cm, $\beta_1 \gtrless 1$, perp. shock; ref.11	
(a) $\beta_1 < 1$; $M < M^*$, unsteady	$10c/\omega_{pe}$ (18 mm)
(b) $\beta_1 \sim 5$; $M_A > M_A^*$, stationary; $M_M \sim 2$	$12c/\omega_{pe}$
$M_M \sim 3$	c/ω_{pi}
(IV) In Italy:	
1. Frascati (Ascoli-Bartoli, Martone); θ-pinch 'CARIDDI', r = 9 cm, $\beta_1 < 1$; ref.5,58	
(a) Perp. steady;	$20c/\omega_{pe}$ (3 mm)
(b) Oblique $M_A < M_A^*$; whistler oscillation	(15 mm)
(V) In U.K.:	
1. Culham (Paul); z-pinch 'TARANTULA'; r = 25 cm, $\beta_1 < 1$, perp. shock; ref.1,2,7,57	
(a) Low, $M_A < M_A^*$; steady, monotonic, conservation T_e	
ion acoustic turb. observed	$7c/\omega_{pe}$ (1·4 mm)
(b) Intermediate, $M_A^* < M_A < 6$; steady double structure	$10c/\omega_{pe}$, $2c/\omega_{pi}$ (15 mm)
(c) High, $M_A \sim 6$; unsteady oscillation	$3c/\omega_{pi}$
Non-classical electron heating demonstrated for all M_A	

TABLE III

DIAGNOSTICS

Process	Parameters	Technique
Initial Plasma	n(relative), T_e	Double Langmuir probe
	$\int n_e \, dl$	Interferometry (visible, I.R., microwave)
	$\int n_n \, dl$	Two λ inteferometry
	n_n	Magnetosonic waves
	n_e	Local microwave interferometer
	n_e , T_e	Spectroscopy
Collapse	Dynamics (B , n)	Magnetic probes, Interferometry
	(i) piston and shock velocity → M_A	
	(ii) Separation, steady	
	(iii) Conservation jumps	
Heating	T_e , T_i	Laser scattering, Particle analysis, Spectroscopy
	(i) Species heated	
	(ii) Conservation jump	
	(iii) Collisionless	
	(iv) ν^*	
Macro-structure	B, n, E	Electric and magnetic probes, Interferometry
	mono, double, oscill. L_s	
Micro-structure	Turbulence $\langle n^2 \rangle$, $\langle E^2 \rangle$	Laser scattering, Emission radiation, Probes

the ions, are heated[7]. Also this observed heating cannot be explained by classical transport coefficients[7]; these are inadequate by two orders of magnitude. The shocks are collisionless. The change to a double structure at $M_A^* \sim 3$ suggests that resistivity (collective) is dominant. An effective collision frequency ν^*, has been obtained from L_s and from the observed electron heating. Forward scattering experiments[57] have demonstrated the presence within the shock front of a micro-instability with frequency nearer ω_{pi} than ω_{pe}. An experiment on this type of shock will be described in detail in Part II.

These monotonic shocks are interpreted as resistive shocks dominated by a collective resistivity from micro-turbulence driven by the current. Until recently the only theory of these streaming instabilitis was for a homogeneous plasma without a magnetic field[34]. On this model, for an isothermal initial plasma, compression would tend to develop electron inertia waves. This development could be limited by either of two mechanisms which heat the electrons;

(a) $v_d > v_{eth}$ would drive the two-stream instability with frequency $\omega \sim \omega_{pe}$ and heat the electrons giving $T_e > T_i$;

(b) classical collisional resistivity at the front of the shock giving $T_e > T_i$.

Once $T_e > T_i$, the ion acoustic instability with $\omega \leqslant \omega_{pi}$ can be driven if $v_d > C_s$.

Kadomsev[35] has calculated the spectrum of turbulence $\langle E^2(\omega, k)\rangle$ resulting from the non-linear phase of the ion acoustic instability. Sagdeev[36] has used this spectrum to derive stochastically an effective collision frequency ν^*. The observed collision frequencies[7] agree well with those predicted by Sagdeev.

More recently Krall[32] has considered the inhomogeneous problem in the presence of a magnetic field. He finds that the appropriate instability is an electron drift instability (universal) driven by a combination of ∇B, ∇n, ExB drifts.

The next important steps towards understanding these shocks will be, on the theoretical side, to combine the universal instability mechanism with the non-linear treatment of turbulence and, on the experimental side, to measure the turbulent spectrum and correlate it with the observed heating and with theories.

8.2 Perpendicular Shock with low β and $M_A > M_A^*$

On the fluid model the resistive shock is expected to develop a viscous sub-shock at the rear for $M_A > M_A^*$. There is no experimental evidence for this happening. On the contrary, experimentally[1,2] at $M_A > M_A^*$, the resistive shock develops a broad foot ($L \sim c/\omega_{pi} \sim r_{ci}$) at the front. There are a number of possible explanations for this

discrepancy, including high β effects; but the most attractive one involves the reflection of ions from the resistive shock[24].

On the single particle model, which is more appropriate when discussing the collisionless ions, ions are reflected from the longitudinal electric field within the shock front. The number of ions reflected depends on the spread of the distribution function (i.e. the temperature), because only ions with certain velocities are reflected. Robson and MacMohan[68] have suggested that a viscous sub-shock at the rear of the resistive shock could produce appreciable ion heating and consequently spread the ion distribution function so that more ions are reflected forwards. These reflected ions then gyrate in the magnetic field acquiring transverse energy before finally passing through the shock. During this forward gyration the requirement of charge neutrality will cause electrons to follow the ions. The magnetic field will follow the electrons, giving rise to the observed foot. The interstreaming of ions in this foot could also give rise to interstreaming instabilities and consequent plasma heating. Experimentally there is anomalous electron heating[7] and some evidence from charge exchange neutrals that ions are counterstreaming in the foot[9].

The interpretation of these high Mach number shocks is not clear either experimentally or theoretically.

8.3. Perpendicular high β Shocks

Experimental data has only recently become available[10,11] and the interpretation is not year clear. There is experimental evidence for appreciable turbulence behind these shocks, and this could be related to the turbulence observed behind the magnetospheric bow shock.

8.4. Oblique low β Shocks

There is clear detailed evidence for a train of forward whistler oscillation in oblique shocks[9,13,58]. In one experiment[13] these shocks have been shown to require collective resistivity for $M_A < M_A^*$ and collective resistivity and viscosity for $M_A > M_A^*$. For $M_A > M_A^*$ the Austin[13] and Novosibirsk[9] results disagree. The latter say that the oblique shock becomes broad and monotonic like a perpendicular shock while the former still get oscillations. No forward oscillations are observed in the flow experiments[8] but appreciable turbulence occurs behind the shock.

8.5. Shock Without Magnetic Field

In the absence of a magnetic field, the ion acoustic dispersion relations should give a backward train of oscillations with $\lambda \sim \lambda_D$ at the ion plasma resonance $\omega \sim \omega_{pi}$. Such oscillations have been observed experimentally[9] but at high amplitude the structure broadens to 10 λ_D, presumably because of some interstreaming instability.

PART II

THE TARANTULA EXPERIMENT

1. INTRODUCTION

The Tarantula experimental programme[1,2,7,57] has covered the formation, propagation and structure of collisionless shocks which propagate perpendicular to a magnetic field through a highly ionized initial plasma of low β (i.e. $\beta < 25\%$) and $\omega_{ce}/\omega_{pe} \ll 1$. The aim is to elucidate the mechanism of energy dissipation in the shock when classical transport processes are ineffective; that is, when the shocks are 'collisionless'.

The shock wave is produced by the cylindrical compression of an initial plasma by a fast linear z-pinch in a quartz tube of large diameter, 0·5 m, and length, 1·0 m. The apparatus, called Tarantula[59], is illustrated in Fig.7. The use of z-pinch, rather than θ-pinch, geometry, and the large diameter distinguish this study from most others on collisionless shocks.

The study will be described in five sections: (i) initial plasma, (ii) dynamics of compression, (iii) macro-structure of the shock, (iv) shock heating, (v) micro-structure of the shock.

2. INITIAL PLASMA

2.1. Axial discharge

The discharge tube is normally immersed in a uniform steady axial magnetic field ($0 < B_z < 2$kG) and filled with hydrogen or deuterium in the range 1–40 mT pressure.

The initial plasma is produced by an oscillatory axial current ($I \sim 100$ kA). At the first current reversal the plasma becomes turbulent and rapidly fills the whole tube. At the third current peak ($t = 170$ μs) the driving voltage is removed and a quiescent reproducible plasma develops as the current decays. The shock is produced in this afterflow, when the current is effectively zero ($t \sim 300$ μs).

2.2. Experimental Methods

The initial conditions for the shock experiment have been carefully documented by three experimental methods.

(1) Double Langmuir probes provide local measurements of number density $n_e(r, z, t)$ and electron temperature $T_e(r, z, t)$.

(2) Infra-red laser interferometry provides an absolute measure of $\int n_e(r, z, t)dz$.

(3) The radial propagation of small amplitude magnetosonic waves has been used to determine the density of neutral hydrogen (n_n). Below a critical frequency ($f_c \sim \frac{1}{2} n_i \sigma_{cx} v_i$),

charge exchange couples both ions and neutrals into the wave motion. The measured wave velocity is then related to the total density ($n_n + n_i$).

2.3. Results

The standard conditions, P_o = 20 mT hydrogen and B_{z1} = 1·2 kG, have been diagnosed in detail. The plasma is axially uniform for 98 cm, and radially uniform for the central 20 cm dia. (Fig.8) with parameters,

$$85\%\ \text{ionized};\quad n_e = 7 \times 10^{20} m^{-3},\ T_e = 1{\cdot}4\ \text{eV},\ \beta_1 = 0{\cdot}04$$

The plasma is reasonably quiescent and reproducible. Experiments have been performed over the ranges $10^{20} m^{-3} < n_{e1} < 10^{21} m^{-3}$; $0 < B_{z1} < 1{\cdot}5$ kG ; $0{\cdot}04 < \beta_1 < \infty$.

The initial plasma appears to be contained axially by a narrow (~ 1 cm) neutral layer on the electrode and radially by the axial magnetic field and a more diffuse neutral layer.

3. DYNAMICS OR COMPRESSION

3.1. Pinch device[59] (see Fig.7)

The fast pinch is produced by discharging a low inductance capacitor bank (20 μF) through 40 spark gap switches (source inductance 14 nH) into the initial plasma (load inductance 30 nH). The capacitor bank is inductively coupled to the discharge electrodes, so that the plasma remains at earth potential and probes can be inserted without high voltage insulation. The inductive coupling also provides an approximately square current pulse. For standard initial conditions the measured parameters are: V_c = 75 or 50 kV; E_z = 62, 32 kV/m, $(dI/dt)_o$ = 1·8, 1·1 TA/s and I_p = 420, 320 kA respectively. Standard pinch conditions refer to V_c = 50 kV.

3.2. Magnetic Field Measurements of Piston and Shock

The axial (B_z) and azimuthal (B_θ) magnetic fields have been measured during the compression by using multiple magnetic probes (7 and 3·5 mm dia.) and single probes down to 0·9 mm outside diameter. The shot to shot and year to year reproducibility is within about ± 15%. The piston collapse velocity (V_p ~ 110 km/s) is greater than the Alfvén velocity and thus drives a cylindrically imploding shock.

The shock front is observed as a very sharp change of B_z which moves with velocity V_s ~ 200–500 km/s in front of, and clearly separated from, the piston. For standard conditions there are three phases of the shock implosion as shown in Fig.9.

The overall dynamics of the collapse for standard conditions is illustrated with the aid of a space-time diagram in Fig.10. The detailed study of shock structure has been made

at $r = 9$ cm, where the shock is steady and in a highly ionized uniform plasma. The shock is well separated in space from the piston and in time from the reflected shock, while still approximately planar.

The angle (θ) between the normal to the shock front and the axial magnetic field has been estimated from simultaneous measurements of the time of arrival of the shock at $r = 9$ cm for different axial positions. For standard conditions, the normal to the plane of the shock is perpendicular to B_{z1} near the centre and $\theta \leq 2^{o}$ for $\pm$ 25 cm away axially. Oblique effects occur only if $\theta \geqslant M_A (m_e/m_i)^{\frac{1}{2}} \sim 3{\cdot}5^{o}$ and can therefore be neglected.

3.3. Comparison with MHD Computation

The dynamics of the collapse, as measured by magnetic probes, has been compared with the predictions of a two-fluid MHD computer calculation[60], based on the known initial conditions of the circuit and plasma. With the normal, binary collision transport coefficients the computed shock structure broadens, becoming comparable with the plasma radius. If viscosity is omitted, the structure then steepens beyond the limit of the computation (cf. Section I.4). These shock structure effects, which disagree with the experimental results, have been removed by introducing into the computation an artificially fixed shock width. The dynamics and energetics of the computation are unaffected by this artifice. The total shock heating ($T_i + T_e$) can be predicted but not the ratio T_i/T_e.

Provided the measured initial total density ($n_i + n_e$) is used, rather than the electron density, good agreement is obtained between experimental and computational magnetic profiles and streak diagrams (Fig.11) for $M_A = 2{\cdot}5$ (and $3{\cdot}7$).

4. MACRO-STRUCTURE OF SHOCK

The macro-structure of electric and magnetic field has been measured by imploding the shock onto small magnetic (0·9 mm) and coaxial electric probes situated at $r = 9$ cm. The latter measures the radial potential (V_r).

Three specific cases of low, intermediate and high M_A are listed in Table IV and profiles are shown in Figs.12-14. The dependence of shock width on (c/ω_{pe}) for low M_A has been checked over a range of parameters, as has the change from low to intermediate M_A structure at $M_A \sim 3$.

For low and intermediate M_A the change of radial potential across the shock accounts for the radial ion motion through the shock, indicating the absence of appreciable heating.

TABLE IV

MACRO-STRUCTURE CLASSIFICATION

Alfvén Mach number	Low 2·5	Intermediate 3·7	High 6·3
B_{z_1} (kG)	1·2	0·75	0·43
n_{e_1} (10^{20} m^{-3})	6·2	5·9	4·0
β_1	0·04	0·10	0·20
Structure	Single, steady	Double, steady	Oscillations, unsteady
L_s (mm)	1·4	1·4 15·0	3·0
L_s	$7c/\omega_{pe}$	$7c/\omega_{pe}$ $2c/\omega_{pi}$	$3c/\omega_{pi}$

The importance of classical collisions can be measured crudely by the ratio of collision time to shock rise time (τ_s). For low M_A, if the ions were heated $\tau_{ii} \gg \tau_s \sim 10$ ns; but if, as described later, the electrons are heated, τ_{ee} is only marginally greater than τ_s for standard conditions. At lower pressures $\tau_{ee} > \tau_s$.

It is possible to solve simplified two-fluid equations of motion through the shock by using the experimental profiles of B_z and V_r. In this calculation it is assumed that the electrons are heated by an effective resistivity, the ions are adiabatic and there is no azimuthal momentum. The computation gives predicted profiles of n_e, v_i, T_e, η^*. The final T_e agrees well with the measurements described in the next section.

5. SHOCK HEATING

5.1. Thomson Scattering of Laser Light

Heating of the electrons has been measured by Thomson scattering[61]. A 400 MW 20 ns light pulse from a ruby laser is passed across the diameter of the discharge tube at the midplane. The laser pulse is timed relative to the shock structure using an electric probe moved azimuthally out of the optical paths. The light, Thomson scattered into the axial direction from a 1 cm length of the laser beam centered at r = 9 cm, is detected by a photomultiplier (Fig.15). The spectral profile of the scattered light is obtained by using interference filters with narrow pass-band (3 to 35 Å) and high rejection ratios ($\sim 10^{-4}$).

This spectral profile, which results from Doppler broadening by the electrons ($k\lambda_D \gg 1$), fits a Gaussian to within ± 15% for over a half width of the profile, and yields an electron temperature with standard deviation of ± 10% (Fig.16). Systematic errors increase the possible error to ± 15%. Calculations, based on these measured temperatures, show that there should be sufficient time for the electrons to thermalize before the measurements.

5.2. Measured Electron Temperatures and Comparison with Computations

The measured electron temperatures (T_e) for $M_A = 2{\cdot}5$ and $3{\cdot}7$ are presented in Fig.17 as a function of time (τ) relative to the sharp transition in the shock structure recorded by the electric probe. For $M_A = 3{\cdot}7$ the change in magnetic field (ΔB_z) is plotted as well to show the measurement of T_e within the broad forward transition in the shock structure.

The electron temperatures in Fig.17 are compared with the total shock heating ($T_e + T_i$) derived (assuming $\gamma = 5/3$) from (i) plane geometry conservation relations, using the measured V_s, n_{e1} and B_{z1}, and (ii) the cylindrical collapse MHD computations[60] based on the initial conditions. This collapse computation has been shown above to give good agreement with the measured dynamics of the experiments and consequently should provide a reasonable estimate of ($T_i + T_e$). This comparison is summarized in Table V.

TABLE V

COMPARISON OF TEMPERATURES (eV)

M_A	2·5	3·7	6·3
T_e measured (peak)	44	56	44
T_e extrapolated to $\tau = 0$	46	66	-
($T_e + T_i$) conservation	42	72	140
($T_e + T_i$) computation	49	84	145

There is good agreement between the measured T_e and the predicted ($T_e + T_i$) immediately behind the shock for $M_A = 2{\cdot}5$, and consequently the ions cannot be appreciably heated in this case. However, for $M_A = 3{\cdot}7$ the measured T_e is less than the predicted ($T_e + T_i$), by some 28%, allowing the possibility of some ion heating.

The possibility of temperature limitation by end effects or impurities was investigated for $M_A = 2{\cdot}5$ in an experiment performed in deuterium at half the number density. The dynamics was the same as for hydrogen ($M_A = 2{\cdot}5$), and so the temperature should be doubled. The measured temperature, $T_e = 91$ eV for $\tau = 50$ ns confirmed this simple scaling and made temperature limitation unlikely.

6. COLLISIONLESS SHOCK

6.1. Inadequacy of Classical Transport Coefficients

The electron heating to be expected from the classical transport coefficients can be calculated from the measured fields. In order to calculate the adiabatic and viscous heating it is necessary to calculate self consistent profiles of $n(x)$ and $v(x)$ through the shock. However, the calculation shows that these effects are secondary to the main resistive heating.

The electron energy equation has the form

$$\frac{3}{2}nk\upsilon\frac{dT}{dx} = -A + V + R$$

(i) adiabatic part $A = nkT_e \frac{d\upsilon_x}{dx}$,

(ii) viscous part $V = \mu_e \left[C_1 \left(\frac{d\upsilon_x}{dx}\right)^2 + C_2 \left(\frac{d\upsilon_y}{dx}\right)^2 \right]$,

where μ_e = electron viscosity[62] $\upsilon_y = -\frac{1}{\mu_o ne}\frac{dB}{dx}$ (M.K.S. units) and C_1 and C_2 are functions of $\omega_e\tau_e$ given by Braginski[62].

(iii) resistive part $R = \frac{\eta}{\mu_o^2}\left(\frac{dB}{dx}\right)^2$

where η is the Spitzer-Härm resistivity. Electron inertial effects have been shown to be negligible because $L_s > (c/\omega_{pe})$. The heat flux vector, which can redistribute but not generate heat, has been omitted. The equation was integrated 'step-wise' on a computer using the observed B_z and V_r profiles.

For $M_A = 2{\cdot}5$ this calculation results in a temperature of only 7·5 eV which is a factor of six down on that observed. Viscous heating is negligible and adiabatic heating some 20% of the total, so that resistivity and the B profile dominate. If the classical resistivity is increased by a factor of about 100 throughout the structure, the observed heating can be obtained. Thus classical resistivity is inadequate, by about two orders of magnitude, to expalin the observed electron heating and a 'collisionless' mechanism is necessary.

Similarly, for $M_A = 3{\cdot}7$ and $6{\cdot}3$ classical heating is inadequate. The ratio (R) of observed to classical heating for the broad and sharp features at $M_A = 3{\cdot}7$ are $R = 6$ and 8 respectively; while for $M_A = 6{\cdot}3$, $R = 10$.

By integrating the simple electron energy equation across the shock, an effective mean resistivity and corresponding collision frequency (ν_M^*) can be obtained from $(T_2 - T_1)$, $(B_2 - B_1)$, V_s and L_s. For both hydrogen (20 mτ) and deuterium (10 mτ) shocks with $M_A = 2{\cdot}5$,

$$\nu_M^* \approx 0{\cdot}5 \times 10^{10}\ s^{-1}$$

6.2. Collisionless Mechanism for low M_A (see Section 8.1)

The most probable mechanism for these shocks is the excitation of electrostatic plasma waves by the drift of electrons through ions in the high current density of the shock transition. This electron motion results from a combination of $\nabla_r B$, $\nabla_r n$ and $E_r \times B_z$ drifts. The instability has the nature of a high frequency universal drift mode[32].

For lack of better theoretical guidance, this problem has often been discussed in terms of the 'drift' instability of a homogeneous plasma carrying a current in the absence of a magnetic field[34]. Two types of instability are considered:

(i) ion acoustic instability arising from a resonance of electrons with ion acoustic waves ($\omega < \omega_{pi}$) for $v_d > C_s$ and $T_e > T_i$,

(ii) two-stream instability arising from resonance of ions with electron plasma waves ($\omega = \omega_{pe}$) for $v_d > v_{eth}$.

The occurrence of these instabilities depends on two ratios, (i) $R_v = v_d/v_{eth}$ and (ii) $R_T = T_i/T_e$, as shown in Fig.18. In the shock problem ($1/\omega_{ce} \ll \tau_s \ll (1/\omega_{ci})$ so that the magnetic field is more likely to affect the resonant electrons of the ion acoustic than the ions of the two stream instability.

The measured magnetic field gradient corresponds to a peak azimuthal current density of 4 kA/cm^2. If it is assumed that the mean density $\frac{1}{2}(n_1 + n_2)$ and mean electron temperature $\frac{1}{2}(T_{e1} + T_{e2})$ occurs at this peak, the resulting ratio of electron drift to thermal velocity

$$R_v = \frac{v_d}{v_{eth}} \approx 10\% \ .$$

Assuming in addition adiabatic compression of the ions with $\gamma = 2$,

$$R_T = \frac{T_i}{T_e} \approx 10\% \ .$$

Such conditions, according to Stringer[34], are unstable to the ion acoustic but not to the two stream instability.

Nevertheless the two stream instability could be present, if (i) the electrons are non-Maxwellian with a high velocity component, or (ii) there is a small unresolved region of high drift velocity.

The ion-acoustic instability by itself cannot provide a self-consistent model because it requires $T_e > T_i$, which is not satisfied at the start of the shock structure. A 'trigger' mechanism is therefore required to raise T_e so that the ion acoustic instability can proceed. Both ordinary resistivity and the two-stream instability have been suggested as trigger mechanisms operating at the front of shock.

The non-linear phase of the ion acoustic instability in a homogeneous unmagnetized plasma has been studied by Kadomtsev[35]. He assumes a constant growth rate at resonance from linear theory and non-linear 'diffusion' in (ω ,k) space produced by scattering of waves on ions. Thermalization of the waves is not considered. From this study he derives

the spectrum, $\langle E^2(k) \rangle$, of the resulting turbulent electric field.

The interaction of electrons with this turbulent electric field gives rise to an effective collision frequency (ν^*) and corresponding turbulent resistivity (η^*), which have been calculated by Sagdeev[36].

$$\nu^* = 10^{-2} \frac{T_e}{T_i} \left(\frac{M_i}{kT_e}\right)^{\frac{1}{2}} v_d \omega_{pi} = 10^{-2} \frac{T_e}{T_i} \frac{v_d}{v_{eth}} \omega_{pe} \, .$$

(Note that this ν^* is 100 times smaller than that given by Sagdeev and Galeev[63].)[4]

Sagdeev also predicts

$$\frac{dT_e}{dT_i} = 43 \frac{v_d}{v_{eth}} \, ,$$

which, for experimental values, agrees with the observed dominance of electron heating. Substitution of mean shock parameters into the equation yielded

$$\nu^* = 1{\cdot}4 \times 10^{10} \ s^{-1}$$

in reasonable agreement with values desrived from experiment (see Section 6.1).

The scaling experiment, using hydrogen and deuterium at constant $M_A = 2{\cdot}5$, has $n_H = 2n_D$, $L_{sH} = (1/2)L_{sD}$, $T_{eH} = (1/2)T_{eD}$, $\nu_H^* = \nu_D^*$ and corresponds to the Sagdeev formula.

The stewise computation of the classical plasma heating through the shock (Section 6.1) showed sufficient electron heating for ion acoustic instability to develop at the front of the shock at the start of the steep gradient. The computation was then continued with the addition of the above turbulent resistivity with its functional dependence. The instability switches off at the end of the steep gradient. The calculated and the observed electron heating agreed when η^* was reduced by a factor 0·6 from that given by Sagdeev. The computed effective collision frequency averaged over the shock width was $\nu^* = 0{\cdot}8 \times 10^{10} s^{-1}$.

While there is circumstantial agreement between the Kadomtsev-Sagdeev theory and experiment, it must be remembered that the assumed conditions do not correspond with experiment.

Recently Krall[32] has developed a linear theory for local stability within a shock front with ∇B, ∇n, $E_r \times B_z$ drifts. Also recently Drummonds and Sloan[64] have criticized Kadomtsev's assumption that ion scattering dominates the non-linear phase.

7. MICRO-STRUCTURE OF SHOCK FROM FORWARD SCATTERING

7.1. Description

Recently direct evidence for the existence of micro-instability within the shock has

---

[4] It appears from recent discussions[70] that the factor 10^{-2} given by Sagdeev[36] was introduced to give better agreement with experiment

been obtained for $M_A = 2{\cdot}5$. Forward scattering of ruby laser light from plasma density fluctuations[61] with wavelength greater than the Debye length (see also Chapter 11 of this book by Ramsden), shows an appreciable enhancement[57] over the stable thermal level, of these fluctuations within the shock front. The enhancement occurs for relatively small frequency shifts from the laser line corresponding to the range of low frequency plasma waves (ion feature). This result reinforces previous suggestions that ion acoustic rather than two stream turbulence dominates in this shock.

A 50 MW laser pulse of half height full width 35 ns was timed and positioned to hit the shock front in the mid-plane of the discharge tube when the shock is at 9 cm radius. The relative timing of the laser pulse to the shock structure was obtained from an electric probe at the same 9 cm radius but moved azimuthally out of the field of view.

The laser beam is in a plane which is tangential to the cylindrical shock front (electric vector perpendicular to this plane) and within this plane is at $2{\cdot}25^{o}$ to the axial direction. The forward scattered light is detected in the same plane at an angle of $4{\cdot}5^{o}$ to the laser beam (Fig.19). The plasma fluctuations which scatter light into this detector have wave vector k colinear with azimuthal current in the shock and $|k| \leq 1/\lambda_D$ (i.e. collective scattering). A back-scattered signal is detected in a slightly different plane at an angle of 170^{o} to the laser beam. This back-scattered light signal arises from fluctuations with $|k| \gg 1/\lambda_D$ (i.e. random thermal fluctuations) and monitors the electron heating. Both detecting systems are focused onto the 2 mm diameter laser beam at the mid-point of the discharge tube.

Spectral resolution of the forward-scattered light was obtained by using optical filters in front of the photomultiplier. A narrow pass-band (3 Å) filter was used to accept light scattered from the low frequency ($\Delta\omega \sim \omega_{pi} \equiv 0{\cdot}1$ Å) fluctuations (ion feature), while rejecting most of the light scattered from the high frequency ($\Delta\omega \sim \omega_{pe} \equiv 7$ Å) fluctuations (electron feature). A wider pass-band (35 Å) filter was used to accept light scattered from both features. Spectral resolution of the back-scattered signal was obtained by using a wide pass-band (30 Å) filter set about 50 Å off the ruby line so that a signal appears only when the electrons are appreciably heated.

7.2. Results

A pulse of forward-scattered power is observed (Fig.20) which is much shorter than the laser emission. This pulse corresponds in time and duration with the passage of the shock front through the laser beam. The rise time of the pulse (5 ns) is just within the limit of the photomultiplier response. Clearly there is no resolution in space or time within the shock front.

The time variation of the ratio of scattered to incident power, hereafter called normalized scattered power, has been derived from Fig.20 and plotted in Fig.21. This illustrates the enhancement of scattering within the shock over that from the pre- and post-shock plasma. With more gain in the detection system the pre- and post-shock scattering can be seen, as in Fig.20, together with the enhancement within the shock seen in the wings of the laser pulse.

The back-scattered power, also shown in Fig.20, is insignificant from the cold initial plasma ($T_e \sim 1{\cdot}4$ eV) but appreciable from the hot post shock plasma ($T_e \sim 45$ eV).

The normalized scattered power from the plasma is not very reproducible. The average of about ten measurements from either the pre-, on, and post-shock regions, gave a standard deviation of about 30%. The average spurious signal (no plasma) was more reproducible, with standard deviation of about 5%. These average measurements of the normalized scattered power, corrected for spurious signal, and relative to pre-shock plasma, are given in Table VI[57], for both 3 Å and 35 Å filters.

Within experimental error, the ratio of peak normalized scattered power from the shock to that from the initial plasma, is the same for both filters, yielding a ratio $R = 16$. This result demonstrates that most of the enhanced scattering from the shock occurs within the ion feature rather than the electron feature.

TABLE IV

	35 Å	3 Å
Pre-shock	1	1
On shock	16	16
Post-shock	2	0·7
Spurious	1·5	1·0

The observed ratio, R, should be corrected for the ratio of scattering volumes. The shock does not occupy the whole cross sectional area of the laser beam, whereas the pre-shock plasma does. For the assumed dimensions and geometry, effective shock thickness ~ 1·4 mm, laser beam ~ 2 mm, this correction raises the ratio to $R = 37$.

7.3. Local Enhancement

The measured ratio, R, is not the true local enhancement relative to what the scattered power in the ion feature would be from a stable plasma with the same parameters. The power in the ion feature from such a stable plasma, with no current, depends on $\alpha = 1/(k\lambda_D)$ and T_e/T_i[61]. Both of these parameters vary through the shock, $4{\cdot}4 > \alpha > 1{\cdot}2$ and $1 < T_e/T_i < 12$ from pre- to post-shock plasma. Unfortunately the theoretical dependence

of the scattering on these parameters for $T_e/T_i > 3$ is not available without computation. Such a computation[65] shows that the total (ion and electron feature) scattering cross section is almost constant for the experimental variation of α and T_e/T_i. However, as the contribution of the electron feature to this total cross section increases through the shock, that of the ion feature must decrease. Thus the local enhancement of the ion feature is greater than the quoted ratio, R, relative to the initial plasma.

The above estimate of the scattering from a similar stable plasma took no account of the electron current drift velocity, the source of instability. According to Rostoker and Rosenbluth[61], the presence of an electron current within a stable plasma produces only a small (< 2) enhancement of the ion feature for up to 90% of the critical current for instability.

The firm conclusion from this discussion of the experimental results is that the observed peak in the forward scattered power cannot be explained without assuming the presence of a microinstability within the shock front.

7.4. Inferred effective collision frequency

It is possible to extend the interpretation of these results onto less certain ground. The measured density fluctuations can be converted into electric field fluctuation, which can then be used to derive an effective electron collision frequency. This latter step involves assuming the k-spectrum of the turbulence and this has not been measured. Nevertheless, it is interesting to consider the consequences of combining theoretical spectra with the observed level of fluctuation at one k value.

The ratio of the scattered signal from the shock (subscripted S) to that from the initial plasma for a given k and within the ion feature is simply the ratio of the Fourier spectral densities of the corresponding plasma density fluctuations within the frequency range of the ion feature:

$$R(k) = \frac{\langle n_e^2(k)\rangle_S}{\langle n^2(k)\rangle_1} .$$

The electric field fluctuation $\langle E^2(k)\rangle$, can be derived from $\langle n^2(k)\rangle$, by assuming the low frequency dispersion relations for ion acoustic waves and an effective mean temperature for the shock.

$$\langle E^2(k)\rangle_S = (\alpha_1/\alpha_S)^4 R(k)\langle E^2(k)\rangle_1 .$$

If the initial plasma is thermal, the Rayleigh-Jeans law and the dispersion relations yield

$$\varepsilon_0 \langle E^2(k) \rangle_1 = kT_{e_1} F(\alpha_1) \quad \text{(M.K.S. Units)}$$

where

$$F(\alpha) = \alpha^2/[(1 + \alpha^2)(1 + 2\alpha^2)] = F(k) \ .$$

However, recently the scattering from the initial plasma has been calibrated absolutely by Rayleigh scattering from nitrogen gas. This has shown that the scattering is a factor $A \approx 40$ above the thermal level. [/] Then

$$\varepsilon_0 \langle E^2(k) \rangle_1 = AkT_{e_1} F(\alpha_1) \ .$$

A test particle with initial velocity u_0 experiences stochastic deflections in a turbulent electric field $\langle E^2(\omega, k) \rangle$. With the usual definition of an effective collision frequency

$$\nu^* = \frac{1}{u_0^2} \frac{\partial}{\partial t} \langle u_\perp^2 \rangle \Big|_{t=0} = \frac{1}{u_0^2} D_\perp \ .$$

The Fokker-Planck perpendicular diffusion coefficient in velocity-space has been evaluated[66,67] in the form

$$D_\perp = \frac{1}{(2\pi)^3} \left(\frac{e}{m} \right)^2 \int \left(1 - \frac{(k \cdot u_0)^2}{k^2 u_0^2} \right) \langle E^2(\omega, k) \rangle \, \delta(\omega + k \cdot v) d^3k d\omega$$

where

$$\langle E^2(\omega, k) \rangle = \int \langle E^2(r, t) \rangle \{ \exp -i(k \cdot r + \omega t) \} dt \ .$$

The form of the collision frequency can be simplified[69] by assuming that the test particle is an electron with the mean thermal velocity (v_{eth}) which is much greater than the ion acoustic wave phase velocity

$$u_0 = v_{eth} \gg (\omega/k)$$

and that the turbulence is isotropic. Then

$$\nu^* = \frac{1}{6\pi^2} \left(\frac{e}{m} \right)^2 \frac{1}{(v_{eth})^3} \int_0^{k\lambda_D = 1} \langle E^2(k) \rangle k dk$$

The limits correspond to the cut-off of collective wave effects above $k = 1/\lambda_D$.

Substitution of various spectral dependencies of $\langle E^2 \rangle$ on k and plasma parameters between the initial and final states, results in a wide range of ν^*, $10^8 - 3 \times 10^{10}$ s^{-1}, which overlaps the value derived from experiment. Two types of spectrum have been used

---

[/] The scattered signals from the pre- and post-shock plasma have been shown to have a spurious origin. Consequently they do not imply supra-thermal fluctuations. This spurious signal does not affect the scattered signal from the shock nor the conclusions of this section.

(a) power law; the highest ν^* is given by the 1/k dependence which corresponds to the Kadomtsev spectrum[35],

(b) thermal spectral dependence $F(\alpha)$; this gives the highest ν^* for the initial temperature.

These results on the interpretation of the forward-scattering experiments are very preliminary and are included as an indication of the importance of the technique. When more detailed measurements of the spectrum are made and the various theoretical assumptions checked, it should be possible to construct a self-consistent model of the turbulent dissipation within the shock.[/]

[/]Such a self consistent model has now been presented[70,71]

REFERENCES

1. J.W.M. PAUL, M.J. PARKINSON, J. SHEFFIELD and L.S. HOLMES. 1965. 7th Int. Conf. Phen. in Ionized Gases (Belgrade) II, 819.

2. J.W.M. PAUL, L.S. HOLMES, M.J. PARKINSON and J. SHEFFIELD. 1965. Nature Lond., 208, 133.

3. A.M. ISKOLDSKII, R.Kh. KURTMULLAEV, Yu.E. NESTERIKHIN and A.G. PONOMARENKO. 1965. JETP, 20, 517.

4. R.Kh. KURTMULLAEV, Yu.E. NESTERIKHIN, V.I. PILSKI and R.Z. SAGDEEV. 1965. I.A.E.A. Culham Conf. II, 367.

5. U. ASCOLI-BARTOLI, S. MARTELLUCI and M. MARTONE. 1965. I.A.E.A. Culham Conf. II, p.275.

6. G.C. GOLDENBAUM and E. HINTZ. 1965. Physics Fluids, 8, 2111.

7. J.W.M. PAUL, G.C. GOLDENBAUM, A. IIYOSHI, L.S. HOLMES and R.A. HARDCASTLE. 1967. Nature Lond., 216, 363.

8. E. PUGH and R. PATRICK. 1967. Physics Fluids, 12, 2579.

9. S.G. ALIKHANOV, N.I. ALINOVSKI, G.G. DOLGOV-SAVELEV, B.G. ESELEVICH, R.Kh. KURTMULLAEV, V.K. MALINOVSKII, R.Yu. NESTERIKHIN, V.I. PILSKII, R.Z. SAGDEEV and V.N. SEMENOV. 1968. I.A.E.A. Novosibirsk Conf., CN-24/A-1.

10. E. HINTZ. 1968. I.A.E.A. Novosibirsk Conf., CN-24/A-2.

11. R. CHODURA, M. KEILHACKER, M. KORNHERR and H. NIEDERMEYER. 1968. Novosibirsk Conf. CN-24/A3.

12. A.W. De SILVA, D.F. DUCHS, G.C. GOLDENBAUM, H.R. GRIEM, E. HINTZ, A.C. KOLB, H.J. KUNZE and I.M. VITKOVITSKY. 1968. I.A.E.A. Novosibirsk Conf., CN-24/A-8.

13. A.E. ROBSON and J. SHEFFIELD. 1968. I.A.E.A. Novosibirsk Conf., CN-24/A-6.

14. D.E.T.F. ASHBY and J.W.M. PAUL. 1959. 4th Intern. Conf. on Ionization Phen. in Gases (Uppsala), IVA, 961.

15. R.G. CRUDDACE. 1967. Thesis, Oxford (R.G. CRUDDACE and M. HILL. Culham Laboratory Report CLM-M 52, 1966,

16. Yu.A. KOLESNIKOV, N.V. FILIPPOV and T.I. FILIPPOV. 1966. Kurchatov Report 18/904 (Culham CTO/8).

17. A.C. KOLB. 1959. 4th Intern. Conf. on Ionization Phen. in Gases (Uppsala) II, IVc, 1021.

18. F.J. FISHMAN, A.R. KANTROWITZ and H.E. PETSCHEK. 1960. Rev. Mod. Phys. 32, 959 (collisionless claim later withdrawn).

19. N.F. NESS, C.S. SCEARCE and J.B. SEEK. 1964. J. Geophys. Res., 69, 3531.

20. J.T. GOSLING, J.R. ASBRIDGE, S.J. BAME, A.J. HUNDHAUSEN and I.B. STRONG. 1968. J. Geophys. Res. 73, 43.

21. P.L. AUER, H. HURWITZ and R.W. KILB. 1961-2. Physics Fluids, 4, 1105; and 5,298.

22. K.W. MORTON, 1964. Physics Fluids, 7, 1800.

23. V.J. ROSSOW. 1965. Physics Fluids, 8, 358.

24. R.Z. SAGDEEV, 1966. Rev of Plasma Physics, 4, 23.

25. C.F. KENNEL and R.Z. SAGDEEV. 1967. J. Geophys. Res., 72, 3303 and 3327.

26. D.A. TIDMAN. 1967. Physics Fluids, 10, 547.

27. H.E. PETSCHEK. 1963. N.A.S.A. Conference on Physics of Solar Flares, Goddard.

28. J.P. WILD. 1968. Conf. on Plasma Instabilities in Astrophysics, Asilomar (private communication). And with K.V. SHERIDAN and K. KAI. Nature Lond., 218, 536.

29. P.A. STURROCK. 1966. Plasma Astrophysics Summer School at Varenna, p.168; and Nature Lond., 211 695.

30. P.A. STURROCK. 1966. Plasma Astrophysics Summer School at Varenna, p.338; and Nature Lond., 211 697.

31. A. HEWISH, S.J. BELL, J.D.H. PILKINGTON, P.F. SCOTT and R.A. COLLINS. 1968. Nature Lond., 217, 709.

32. N. KRALL. Private communication.

33. R. COURANT and K.O. FRIEDRICKS. 1948. Supersonic Flow and Shock Waves. Interscience.

34. T.E. STRINGER. 1964. J. Nucl. Energy. C, 6, 267.

35. B. KADOMTSEV. 1965. Plasma Turbulence. Academic Press.

36. R.Z. SAGDEEV. 1967. Proc. Symp. in Applied Maths, XVIII, 281.

37. F. De HOFFMAN and E. TELLER. 1950. Phys. Rev., 80, 692.

38. J.E. ANDERSON. 1963. MHD Shock Waves. M.I.T.

39. K.I. GOLDEN, H.K. SEN and Y.M. TREVE. 1961. Fifth Conf. Ionization Phen. in Gases, 2, 2109.

40. L.C. WOODS, 1969. Plasma Physics, 11, 25.

41. P.N. HU. 1966. Physics Fluids, 9, 89. (Later paper by GRAD and HU)

42. W. MARSHALL. 1955. Proc. Roy. Soc. A, 233, 367.

43. J.D. JUKES. 1957. J. Fluid Mech., 3, 275.

44. V.D. SHAFRANOV. 1957. JETP, 5, 1183.

45. W. GEIGER, H.J. KAEPPELER and B. MAYSER. 1962. Nuclear Fusion, Supplement, 2, 402.

46. R.J. BICKERTON, A.E. ROBSON and L.C. WOODS. Private communications.

47. O. BUNEMAN. 1964. Phys. Fluids, Suppl., p.S4.

48. C. SMITH and J. DAWSON. 1963. Princeton Report MATT - 151.

49. E.G. HARRIS. 1968. Lectures at this Summer School (chapter 4).

50. D.W. ROSS. Univ. Texas Report ORO - 3458 - 12.

51. G.M. WALTERS and E.G. HARRIS. 1968. Physics Fluids, 11, 112.

52. S.P. ZAGORODNIKOV, L.I. RUDAKOV, G.E. SMOLKIN and G.V. SHOLIN. 1965. 7th Int. Conf. Phen. in Ionized Gases (Belgrade) II, 791, and Kurchatov Report I.A.E. 909 (Culham CTO/355, 1967).

53. S.P. ZAGORODNIKOV, G.E. SMOLKIN and G.V. SHOLIN. 1966-7. Kurchatove Report I.A.E. 1263. (1966) (Culham CTO/356, 1967).

54. G.C. GOLDENBAUM, 1967. Physics Fluids, 10, 1897.

55. A.W. De SILVA and J.A. STAMPER. 1967. Phys. Rev. Lett., 19, 1027.

57. J.W.M. PAUL, L.S. HOLMES, R.A. HARDCASTLE and C.C. DAUGHNEY. 1968. I.P.P.S. Conf. on Plasma Diagnostics. Culham.

58. M. MARTONE. 1966. Phys. Letters, 22, 73.

59. W.R. BELL, A.E. BISHOP, H.J. CRAWLEY, G.D. EDMONDS, J.W.M. PAUL and J. SHEFFIELD. 1966. Proc. I.E.E. (London), 113, 2099.

60. K. HAIN, K.V. ROBERTS and D.L. FISHER. Private communication.

61. M.N. ROSENBLUTH and N. ROSTOKER. 1962. Physics Fluids, 5, 776.

62. S.I. BRAGINSKI, 1963. Rev. of Plasma Physics, Vol.I. Consultants Bureau.

63. R.Z. SAGDEEV and A.A. GALEEV. 1966. Trieste Lecture on Non-Linear Theory.

64. W.E. DRUMMOND and M.L. SLOAN. Private communication.

65. D.R. MOORCROFT. 1963. J. Geophys. Res., 68, 4870.

66. W.B. THOMPSON and J. HUBBARD. 1960. Rev. Mod. Phys. 32, 714.

67. A.G. SITENKO. 1967. Electromagnetic Fluctuation in a Plasma. Academic Press.

68. A.E. ROBSON and A.B. MacMOHAN. Private Communication.

69. R.S. BICKERTON and I. COOK. Private Communication.

70. E.S.R.I.N. Conference on Collision-free Shock Waves in the Laboratory and in Space, Frascati, 1969. (To be published)

71. J.W.M. PAUL, C.C. DAUGHNEY and L.S. HOLMES. To be published in Nature 1969, Culham preprint CLM-P 201

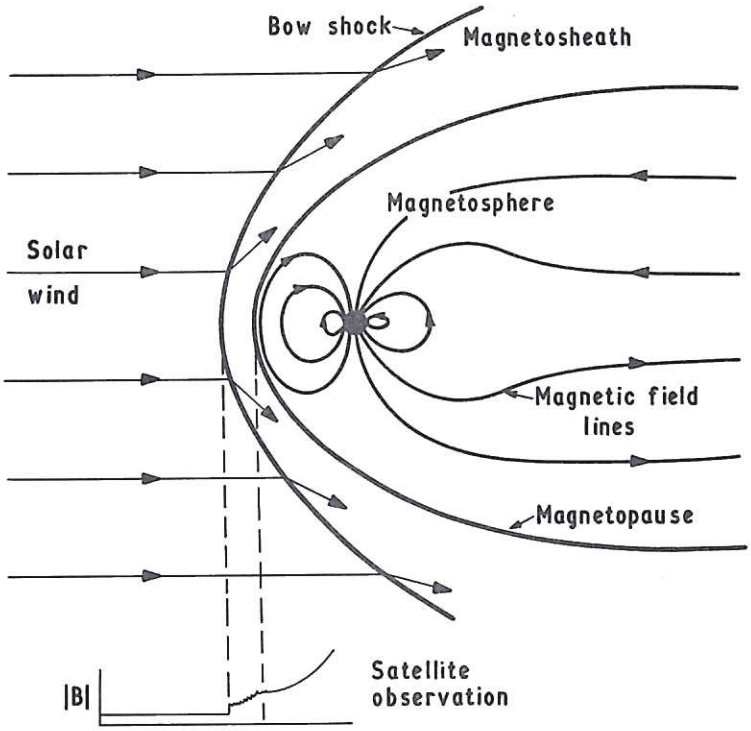

Fig. 1 Schematic of magnetospheric bow shock

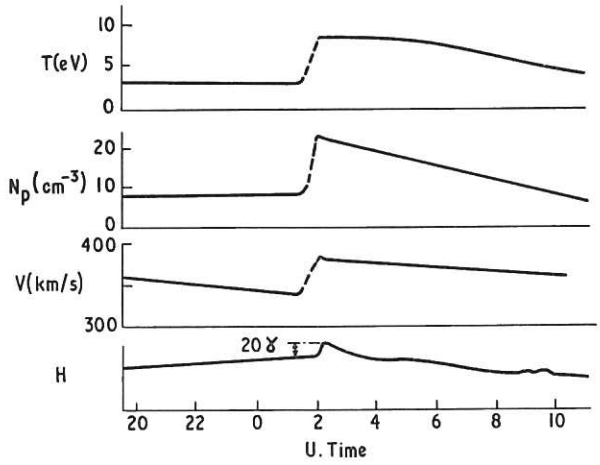

Fig. 2 Interplanetary shock observed by VELA 3A satellite and at Guam on the earth, 19th - 20th Jan. 1966 (Ref. 20)

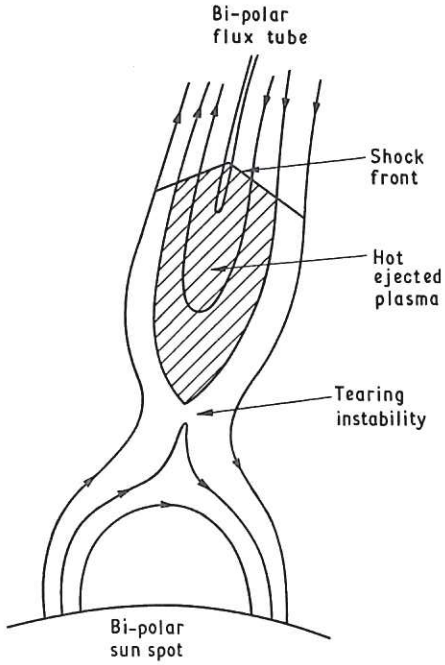

Fig. 3 A model of a solar flare proposed by Sturrock (Ref. 29) with a prominent shock front

CLM - P 218

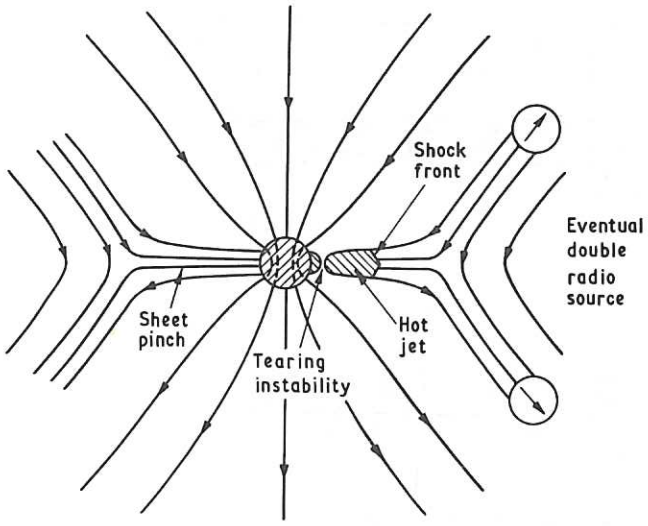

Fig. 4 A model of galactic radio sources proposed by Sturrock (Ref. 30) Gravitational collapse with a magnetic field leads to a tearing instability similar similiar to Fig. 3

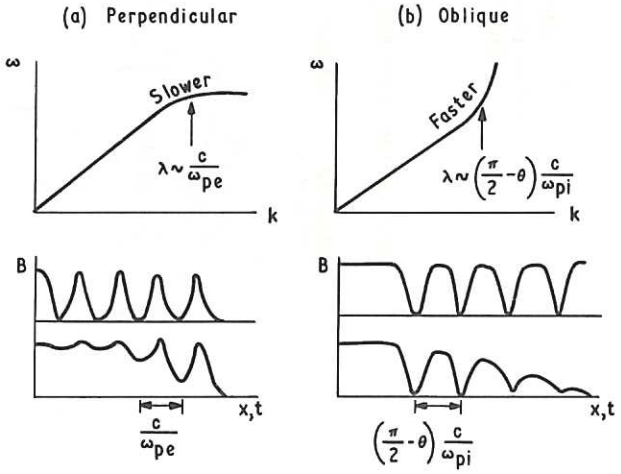

Fig. 5 Dispersion effects (a) Backward wave train, e.g. perpendicular propagation and electron inertia waves. (b) Forward wave train, e.g. oblique propagation and whistler waves.

Fig. 6 Nature of end point singularities of shock jump

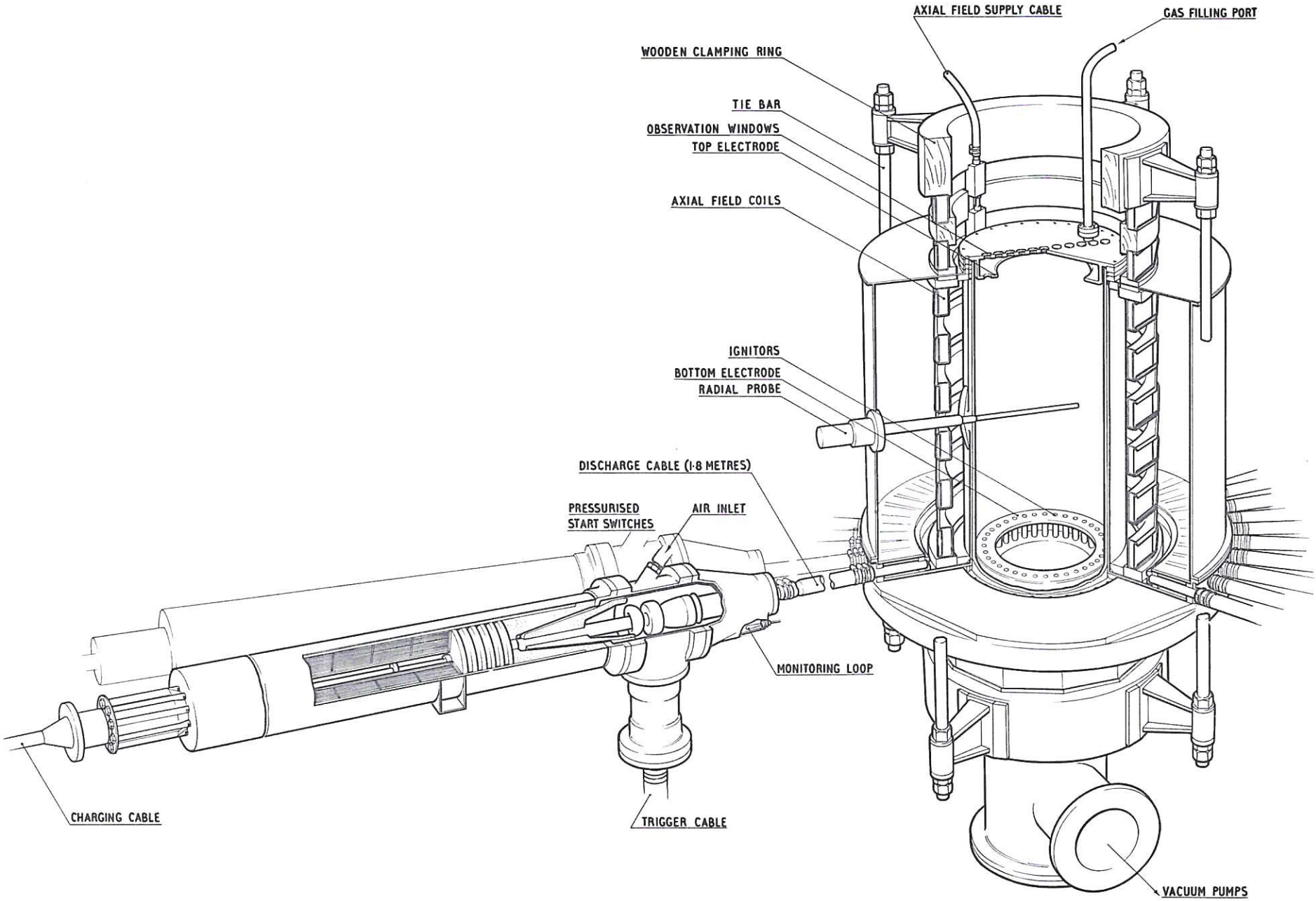

Fig. 7 Main features of the TARANTULA experiment

CLM - P218

ELECTRON DENSITY IN INITIAL PLASMA

(350 μsec AFTER START)

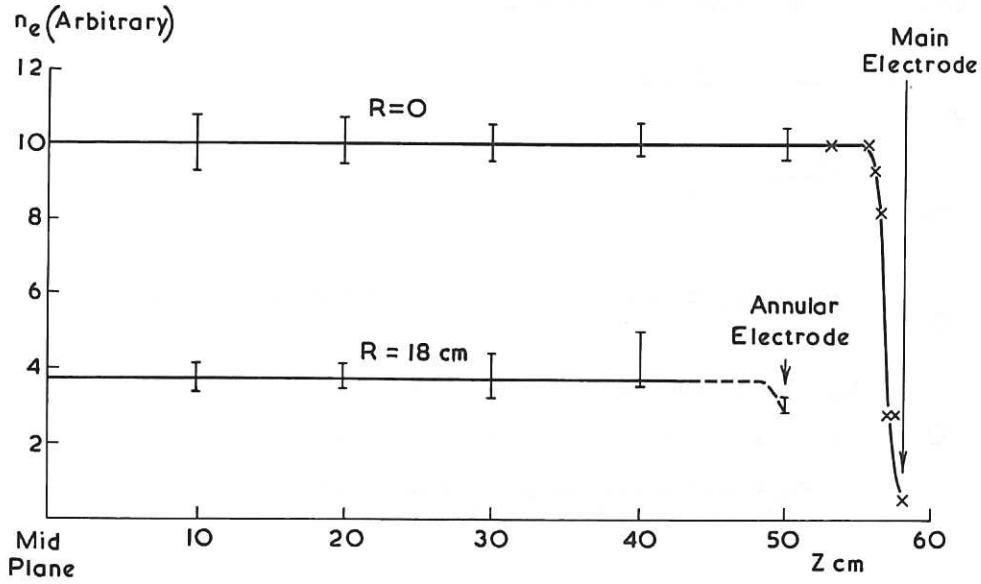

AXIAL VARIATION OF ELECTRON DENSITY

(DOUBLE LANGMUIR PROBE)

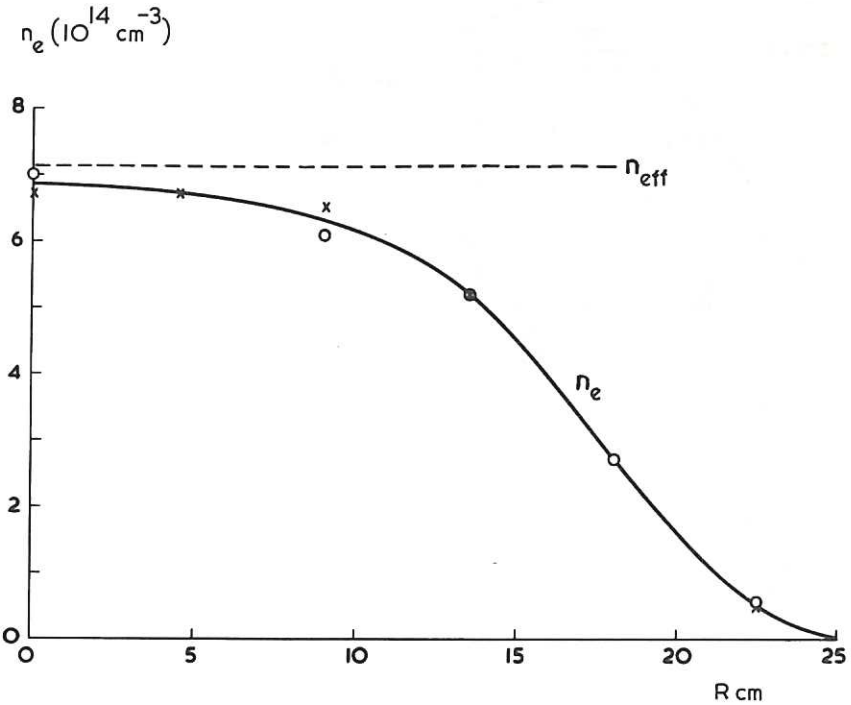

RADIAL VARIATION OF ELECTRON AND TOTAL DENSITY

(O DOUBLE LANMUIR PROBE; X INFRA-RED INTERFEROMETER;
$---\ n_{eff} = n_e + fn_n$, MAGNETOSONIC WAVE 360 kH_z, $f \sim 1$)

Fig. 8 Density distribution in the initial plasma

CLM-P218

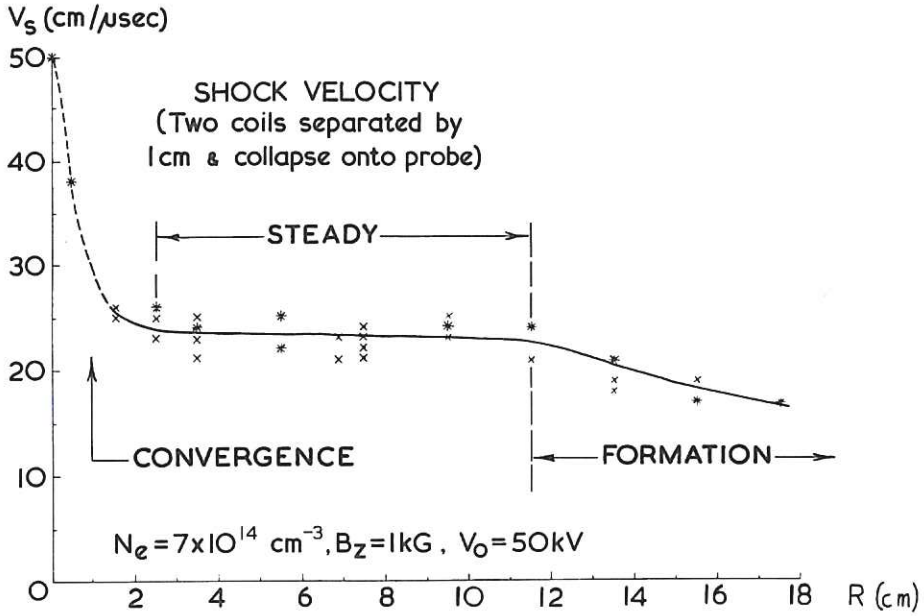

Fig. 9 Radial variation of shock velocity for standard conditions, $M_A = 2.5$, in hydrogen

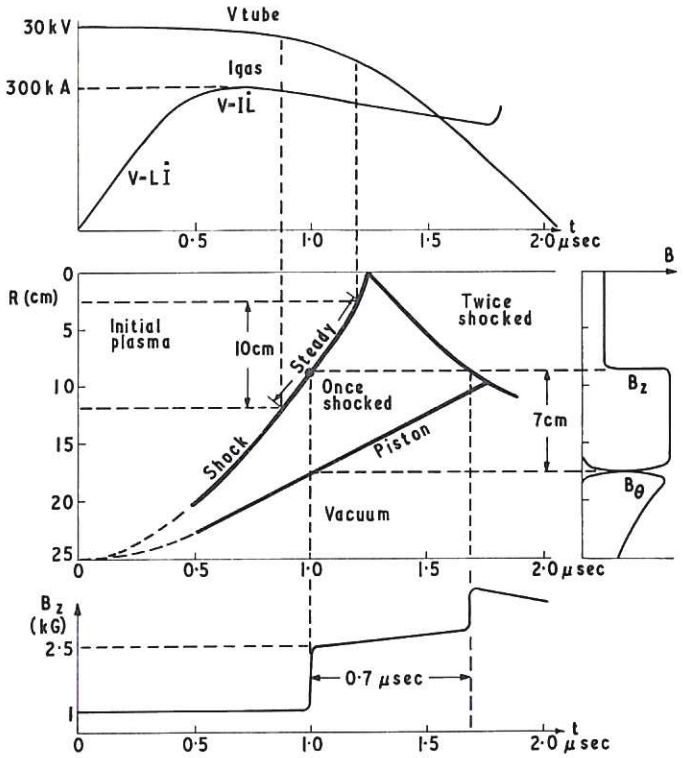

Fig. 10 Schematic of dynamics for standard conditions, $M_A = 2.5$

CLM - P 218

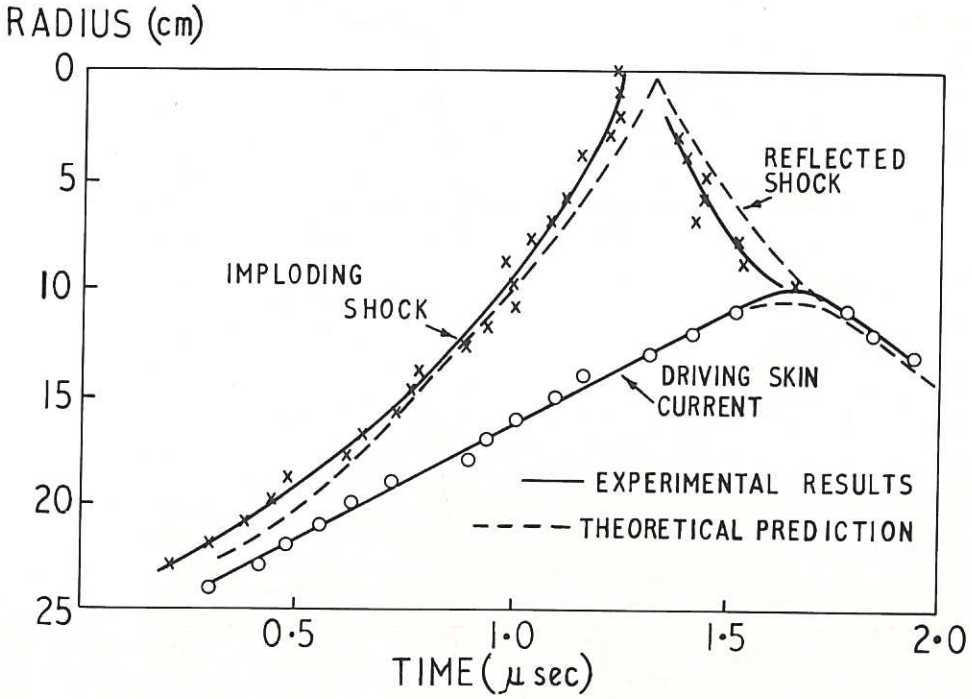

Fig. 11 Comparison of experimental and theoretical dynamics for standard conditions, $M_A = 2.5$

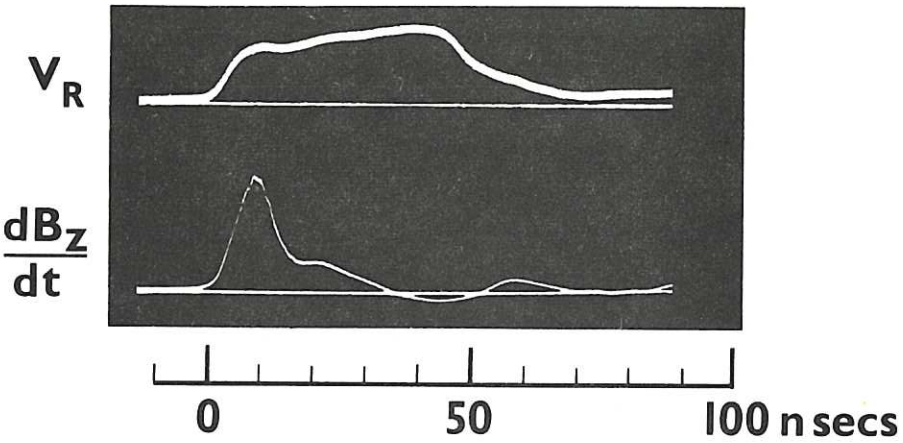

Fig. 12 Oscillograms of radial potential, V_R (1cm separation coaxial probe) and dB_z/dt for standard conditions, $M_A = 2.5$

CLM-P218

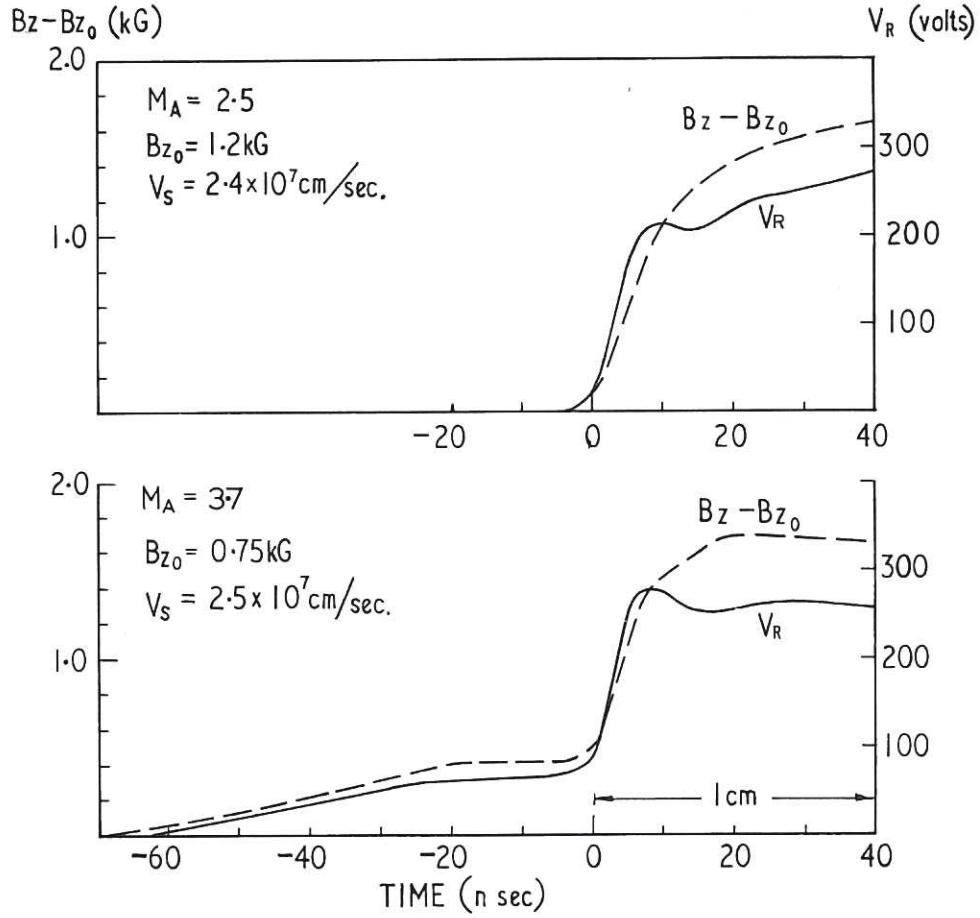

Fig. 13 Structure of V_R and B_z for low and intermediate M_A

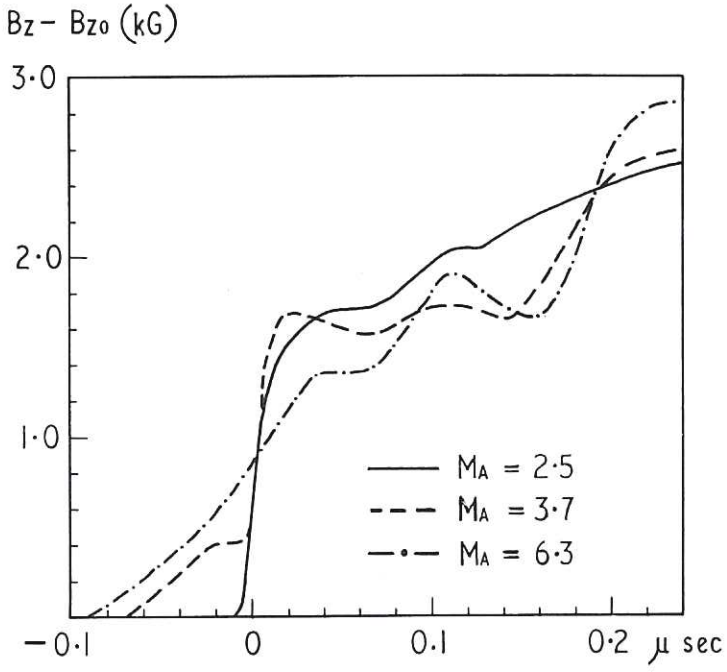

Fig. 14 Structure of B_z for low, intermediate and high M_A

CLM-P218

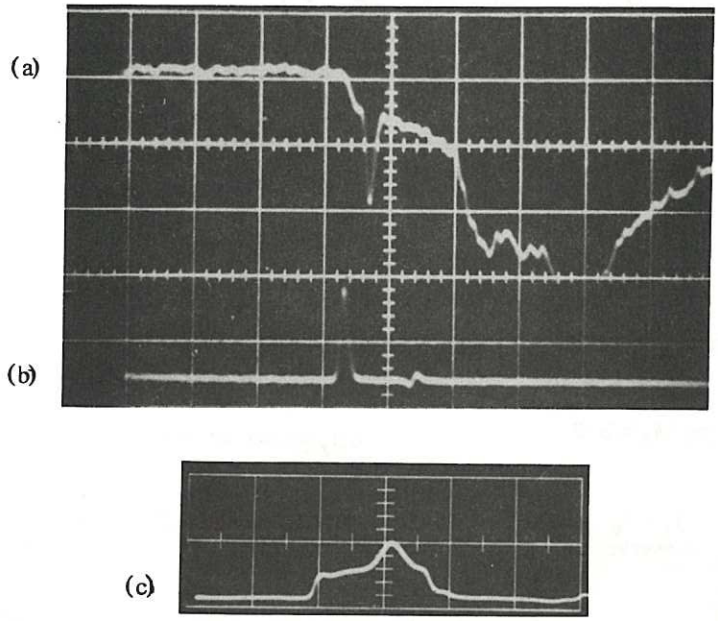

Fig. 15 (a) Scattered light signal with 15 Å wide optical filter set at 6824 Å ($\Delta\lambda \simeq 120$ Å). The sharp rise of background light just before the scattered signal corresponds to the arrival of the shock at the point; (b) Photodiode monitor of input laser power (350 MW); (c) Accurate timing of measurement relative to electric probe signal. The delay of 60 nsec corresponds to 1.5 cm behind the shock.

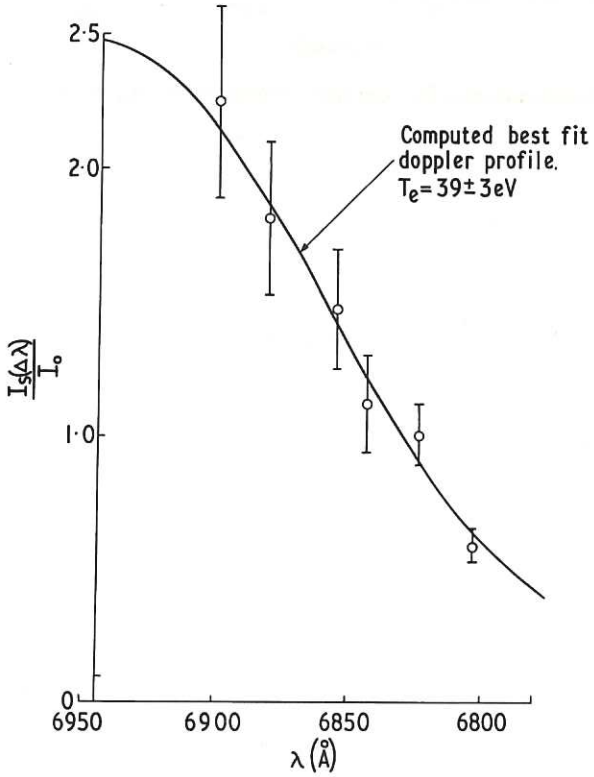

Fig. 16 Plot of ratio of scattered to incident power against wavelength with best fit Doppler profile.

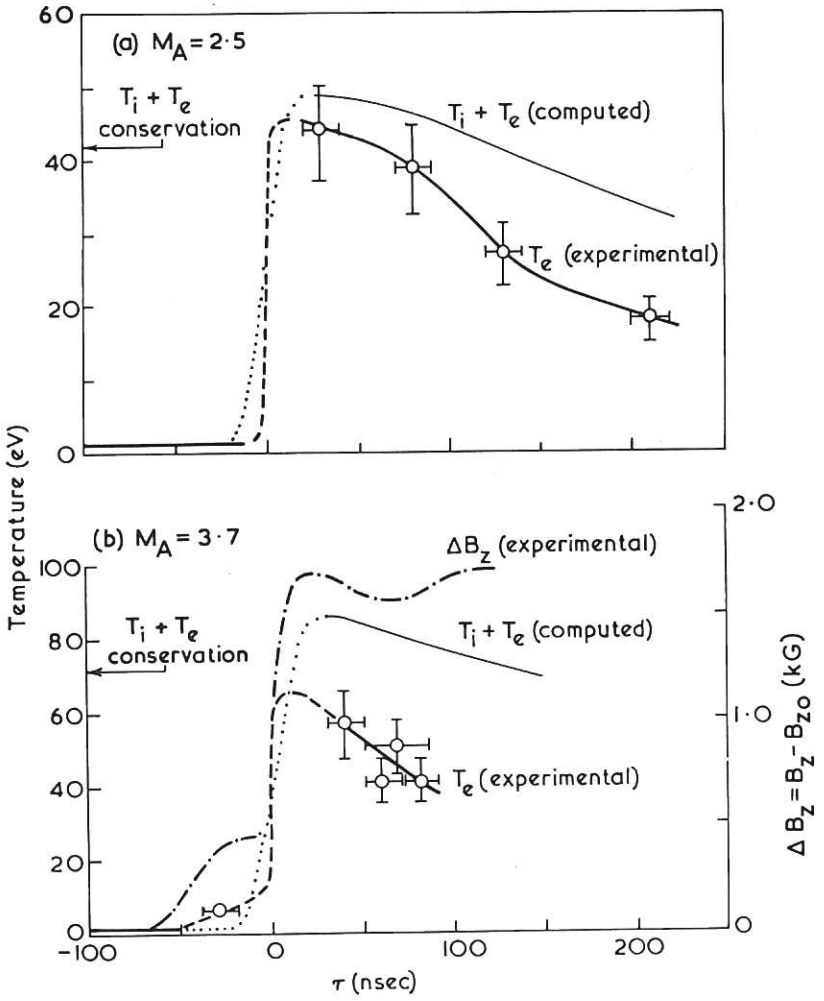

Fig. 17 Temperatures for low and intermediate M_A shocks in hydrogen

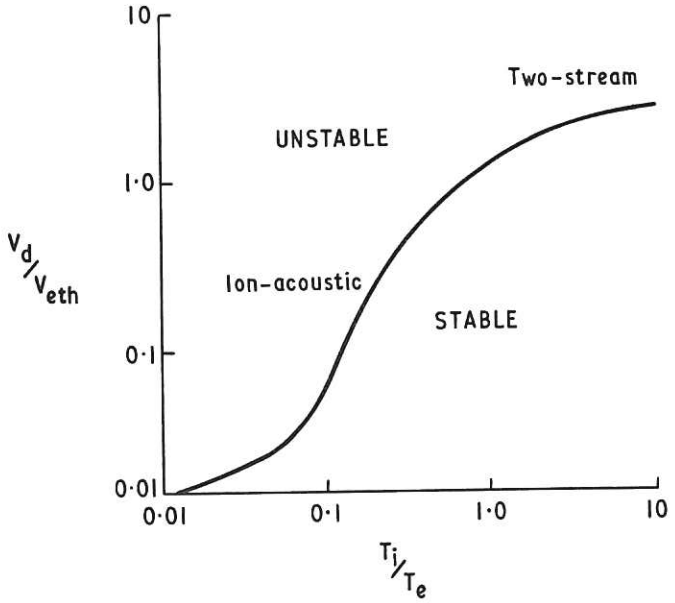

Fig. 18 Current driven streaming instability after Stringer (Ref. 34)

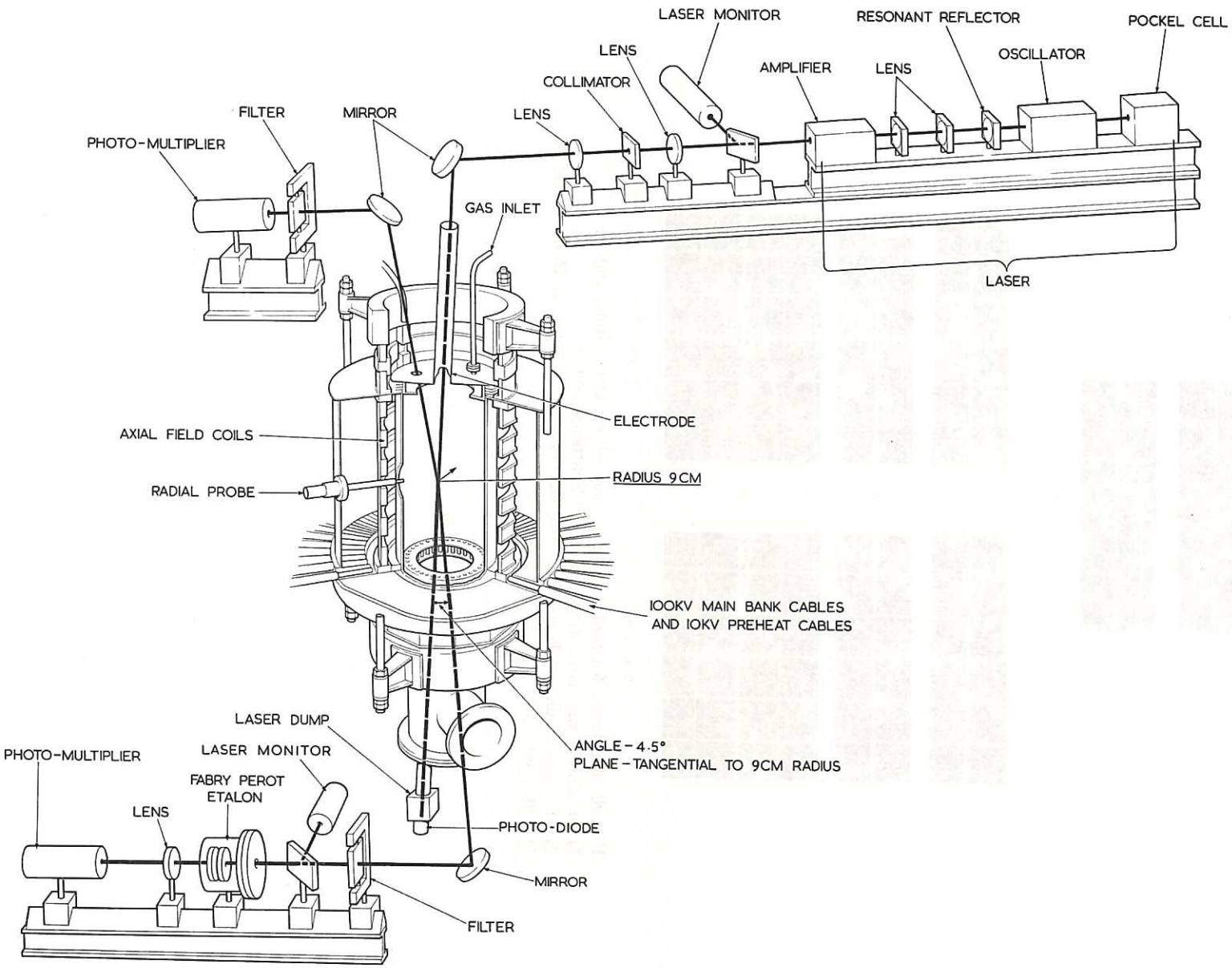

Fig. 19 Experimental arrangement for simultaneous forward and backward scattering
(Note: Fabry-Perot interferometer was not used in reported experiments)

CLM-P218

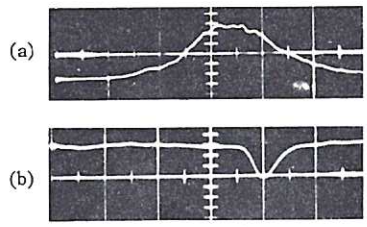

1. On shock

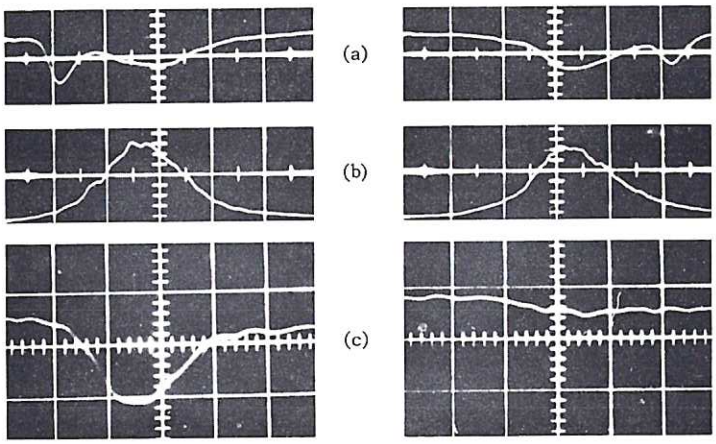

2. Post-shock 3. Pre-shock

Fig. 20 Enhanced forward scattering from shock front (20ns/cm)
1) On shock only, (a) Laser power (b) Scattered power
2) With pre-shock, (a) Forward scattered (b) Laser power (c) Back scattered
3) With post-shock, (a),(b) and (c) as for 2).

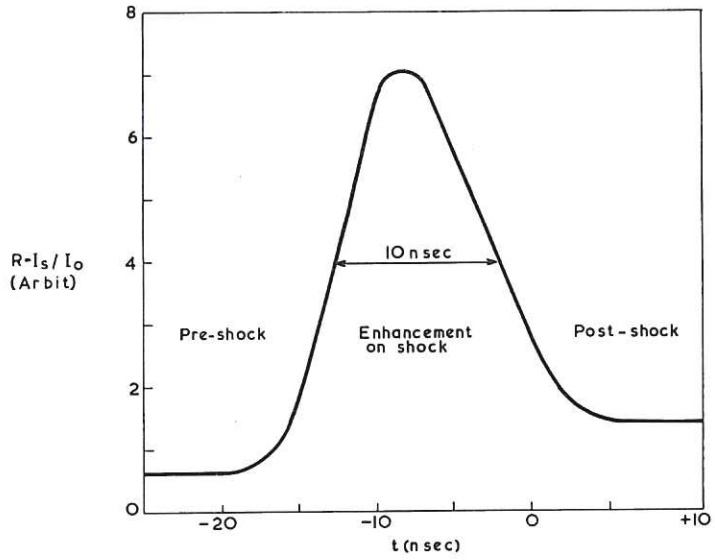

Fig. 21 Normalized scattered power derived from the oscillogram Fig. 20(a).

CLM-P218